

1 **Seasonal variations of ultrafine and sub-micron aerosols in Taipei,**
2 **Taiwan: implications for particle formation processes in a subtropical**
3 **urban area**

4
5 **Cheung, H. C.¹, Chou, C. C.-K.^{1,*}, Chen, M.-J.¹, Huang, W.-R.¹, Huang, S.-H.¹,**
6 **Tsai, C.-Y.¹, Lee, C. S. L.²**

7 1. Research Center for Environmental Changes, Academia Sinica, Taipei 11529,
8 Taiwan

9 2. Institute of Occupational Medicine and Industrial Hygiene, College of Public
10 Health, National Taiwan University, Taipei, Taiwan

11
12 **Correspondence to: C. C.-K. Chou (ckchou@rcec.sinica.edu.tw)*

13
14 **Abstract**

15 The aim of this study is to investigate the seasonal variations in the physicochemical
16 properties of atmospheric ultrafine particles (UFPs, $d \leq 100\text{nm}$) and submicron
17 particles (PM_{10} , $d \leq 1\mu\text{m}$) in an East-Asian urban area, which are hypothesized to be
18 affected by the interchange of summer and winter monsoons. An observation
19 experiment was conducted at the TARO (Taipei Aerosol and Radiation Observatory),
20 an urban aerosol station in Taipei, Taiwan, from October 2012 to August 2013. The
21 measurements included the mass concentration and chemical composition of UFPs
22 and PM_{10} , as well as the particle number concentration (PNC) and number size
23 distribution (PSD) with size range of 4-736 nm. The results indicated that the mass
24 concentration of PM_{10} was elevated during cold seasons with a peak level of $18.5 \mu\text{g m}^{-3}$
25 in spring, whereas the highest UFPs concentration was measured in summertime
26 with a mean of $1.64 \mu\text{g m}^{-3}$. Moreover, chemical analysis revealed that the UFPs and
27 PM_{10} were characterized by distinct composition; UFPs were composed mostly of
28 organics, whereas ammonium and sulfate were the major constituents in PM_{10} . The
29 seasonal median of total PNCs ranged from $13.9 \times 10^3 \text{ cm}^{-3}$ in autumn to 19.4×10^3
30 cm^{-3} in spring. Median concentrations for respective size distribution modes peaked
31 in different seasons. The nucleation mode PNC (N_{4-25}) peaked at $11.6 \times 10^3 \text{ cm}^{-3}$ in
32 winter, whereas the Aitken mode (N_{25-100}) and accumulation mode ($N_{100-736}$) exhibited
33 summer maxima at 6.0×10^3 and $3.1 \times 10^3 \text{ cm}^{-3}$, respectively. The change in PSD
34 during summertime was attributed to the enhancement in the photochemical
35 production of condensable organic matter that, in turn, contributed to the growth of
36 aerosol particles in the atmosphere. In addition, clear photochemical production of
37 particles was observed, mostly in summer season, which were characterized by
38 averaged particle growth and formation rates of $4.0 \pm 1.1 \text{ nm h}^{-1}$ and $1.4 \pm 0.8 \text{ cm}^{-3} \text{ s}^{-1}$,

39 respectively. The prevalence of new particle formation (NPF) in summer was
40 suggested as a result of seasonally enhanced photochemical oxidation of SO₂ that
41 contributed to the production of H₂SO₄, and low level of PM₁₀ ($d \leq 10\mu\text{m}$) that served
42 as the condensation sink. Regarding the sources of aerosol particles, correlation
43 analysis upon the PNCs against NO_x revealed that the local vehicular exhaust was the
44 dominant contributor of the UFPs throughout the year. On the contrary, the Asian
45 pollution outbreaks had significant influence in the PNC of accumulation mode
46 particles during the seasons of winter monsoons. The results of this study implied the
47 significance of secondary organic aerosols in the seasonal variations of UFPs and the
48 influences of continental pollution outbreaks in the downwind areas of Asian
49 outflows.

50 **1. Introduction**

51 Due to the significant impact of particulate matter on human health and climate
52 change, it is vital to understand the formation process of atmospheric particles
53 (Charlson et al., 1992; Donaldson et al., 1998). A number of mechanisms have been
54 proposed by which atmospheric particles are formed, including binary nucleation,
55 ternary nucleation and ion-induced nucleation for charged particles, under different
56 environment conditions (Kulmala 2003; Kulmala et al., 2004, 2012). Numerous
57 studies have been conducted in different locations to elucidate particle formation
58 processes under various environmental settings in the free troposphere, boreal forest
59 and coastal areas, where new particles formation processes are observed frequently
60 (Kulmala et al., 2004, Holmes 2007). Recently, investigations were also carried out on
61 new particle formation within urban boundary layer (e.g., Cheung et al., 2013 and
62 references therein), where particle formation was suggested to be mainly influenced
63 by the photo-oxidation of SO₂. Furthermore, formation of particulate matter by
64 heterogeneous reactions of gases on dust particles was reported recently (Hsu et al.,
65 2014, Nie et al., 2014). Previous investigations have indicated that the air pollutants,
66 in both gaseous and particulate form, associated with the continental outflows of air
67 masses could have affected a wide region in East Asia and caused severe regional air
68 pollution (e.g., Lin et al., 2004; Wang et al., 2003; Buzorius et al., 2004). However,
69 the formation processes of ultrafine particles (UFPs, $d \leq 100\text{nm}$) and sub-micron
70 particles (PM₁, $d \leq 1\mu\text{m}$) under the influences of continental outflows are not yet well
71 understood.

72

73 In urban environment, major contributing sources of aerosol particles include
74 vehicular exhausts (e.g., Pey et al., 2008; Pérez et al., 2010), industrial emissions
75 (Gao et al., 2009) and new particle formation by photochemical reactions (e.g., Pey et
76 al., 2009). Approximately 55-69% of the total particle number concentrations (PNCs)
77 were attributed to secondary aerosols during midday in several European cities
78 (Reche et al., 2011). In Taipei, Taiwan, a subtropical urban area, Cheung et al. (2013)
79 observed that there was a ten-fold increase in nucleation mode particle number
80 concentration (N₉₋₂₅, with size $9 < d < 25\text{nm}$) during new particle formation events
81 compared to that contributed by the vehicle emission. Besides the local sources, air
82 quality of East Asian countries is also strongly affected by the transport of air
83 pollutants from mainland China during periods of winter monsoons (Cheung et al.,
84 2005; Lin et al., 2004; Matsumoto et al., 2003). Lin et al. (2004) reported that the
85 mass concentration of particulate matter (PM₁₀) due to the long-range transport
86 associated with winter monsoons was $85 \mu\text{g m}^{-3}$, about 79% higher than that due to
87 local pollution ($\sim 47.4\mu\text{g m}^{-3}$) in urban Taipei. Chemical composition of fine and

88 coarse particles was measured during a winter monsoon period at Rishiri Island, near
89 the northern tip of Japan, to study the transport of continental aerosols (Matsumoto et
90 al., 2003). The results showed that higher levels of particle mass concentration were
91 associated with the outbreaks of continental polluted air masses. In addition, Cheung
92 et al. (2005) found deterioration in visibility around the southern China during
93 wintertime as indicated by a two-fold increase in aerosol light scattering coefficient
94 under the influences of winter monsoons. Chen et al. (2013) conducted a
95 measurement of the particle number concentration at the background station on the
96 mountain of central Taiwan in summer 2009 and autumn 2010. The result showed that,
97 on the contrary, particle number concentrations were dominated by local sources
98 rather than long-range transport. To date, most of the relevant studies mentioned
99 above were limited to measurements in terms of PM_{10} or $PM_{2.5}$ for a particular period.
100 The seasonal variations of particles in either ultrafine or sub-micron range have not
101 been well illustrated.

102

103 A 1-year aerosol characterization experiment was conducted in the urban area of
104 Taipei, Taiwan. The aim of this study is to attain a better understanding of the
105 seasonal variations of ultrafine and sub-micron particles and the factors affecting
106 particle formation, particularly under the influences of Asian monsoon circulations. In
107 this study, we analyzed number concentration and size distribution of aerosol particles,
108 together with the mass concentration and chemical composition of UFPs and PM_1
109 measured during four seasonal campaigns (i.e. 24 Oct – 15 Nov 2012, 4 – 24 Jan, 17
110 Mar – 11 Apr, and 1 – 14 Aug 2013). The results of this study will contribute to the
111 management strategies of the severe air pollution over the East Asia region.

112

113 **2. Methodology**

114 **2.1 Observation site and instrumentation**

115 The measurements were conducted at the Taipei Aerosol and Radiation
116 Observatory (TARO, 25.02 N, 121.53 E), located in the downtown area of Taipei,
117 Taiwan, during October 2012 to August 2013. The measurements were carried out for
118 2 – 3 weeks in each season (see **Table 1** for measurement details). The aerosol
119 observatory locates on the top floor of the Building-B of the Department of
120 Atmospheric Sciences, National Taiwan University (ASNTU), which is ~20 m above
121 ground level (Cheung et al., 2013).

122

123 Particle number size distribution (PSD) in the range of 4 – 736 nm was measured
124 by two scanning mobility particle sizer (SMPS) systems. One was equipped with a
125 long-differential mobility analyzer (long-DMA, Model: TSI 3081, TSI Inc.) and a

126 condensation particle counter (CPC) (Model: TSI 3022A, TSI Inc.) to measure the
127 particles from 10 – 736 nm, which was named long-SMPS. Another one was equipped
128 with a nano-DMA (Model: TSI 3085, TSI Inc.) and an ultrafine water-based CPC
129 (UWCPC, Model: TSI 3786, TSI Inc.) to measure the particles from 4 – 110 nm,
130 which was named nano-SMPS. The poly-disperse particles were classified into
131 selected mono-disperse particles according to their electrical equivalent mobility by
132 the DMAs. The number concentration of the mono-disperse particles was then
133 counted by the CPCs. Ambient air was drawn into the SMPS systems from outside the
134 building through a 0.635 cm (inner diameter) conductive tube, and a sampling
135 duration of 5 min was adopted for each PSD measurement. The SMPS systems' flow
136 rates were checked weekly during the sampling period and the accuracy of the particle
137 sizing of the DMAs was checked using polystyrene latex (PSL) spheres before the
138 campaigns. Operation details are referred to Cheung et al. (2013).

139

140 Size segregated aerosol samples were collected by a pair of Micro-Orifice
141 Uniform Deposition Impactors (MOUDI, Model: 110, MSP Corp.). Taking the
142 advantage that the cut diameter of the 9th MOUDI impaction stage was exactly 100
143 nm, the 10th impaction stage (cut diameter = 56 nm) of each MOUDI was removed to
144 allow the after filter function as a collector of UFPs (Marple et al., 1991). The
145 sampling flow rate of MOUDI sampler was 30 lpm. Besides, a pair of PM₁ samplers,
146 each consisted of a standard aerosol sampler (PQ-200, BGI Inc.) and a PM₁ sharp cut
147 cyclone, were deployed to collect PM₁ samples with 16.7 lpm sampling flow rate. For
148 both UFPs and PM₁ sampling arrangements, one of the paired samplers was equipped
149 with Teflon filters, whereas another was equipped with quartz fiber filters. The Teflon
150 filter samples were used for gravimetric measurement. The quartz filter samples were
151 deployed for analysis of soluble ions (Na⁺, NH₄⁺, K⁺, Ca²⁺, Mg²⁺, Cl⁻, NO₂⁻, NO₃⁻,
152 SO₄²⁻) using ion chromatograph (IC), and carbonaceous components (i.e. organic
153 carbon, OC and elemental carbon, EC) in the aerosols using a DRI-2001A
154 carbonaceous aerosol analyzer with IMPROVE-A protocol (Chow et al., 2007).
155 Details of the in-lab analysis are as described previously (Salvador and Chou, 2014).
156 Both the PM₁ and UFPs were collected with double-layered quartz filters (i.e. QBQ
157 setup) and the artifacts due to adsorption of gaseous components were corrected as
158 suggested by Subramanian et al. (2004). The sampling duration of each sample set
159 (for both MOUDI and PQ-200 samplers) was from 14:00 - 12:00 LT (22 hr), and a
160 total of 69 and 75 sets of UFPs and PM₁ samples were collected during the entire
161 investigation period (sample sets collected in autumn, winter, spring and summer
162 were 20, 15, 25, and 9 sets for UFPs, and 21, 16, 25, and 13 sets for PM₁,
163 respectively).

164

165 Moreover, to assist the data interpretation, the hourly averaged mass
166 concentration of PM₁₀, the mixing ratio of trace gases (i.e. NO_x, SO₂ and O₃) and the
167 meteorology parameters (i.e. wind direction/speed and UVB (wavelength: 280 - 315
168 nm)) from the Guting air quality station of Taiwan Environmental Protection Agency,
169 which is about 1 km from the TARO, were analyzed in this study. The details of
170 instrumentation setup for trace gas measurements are referred to Cheung et al. (2013).

171

172 **2.2 Data processing and analysis**

173 The PSD of 4 – 736 nm presented in this study was combined from two sets of
174 SMPS data, where the nano-SMPS corresponded to the size range of 4 – 50 nm, and
175 the long-SMPS corresponded to the size > 50 nm. The diffusion loss of the particles
176 during the sample transport in the tubing was corrected according to the algorithm
177 proposed by Holman (1972). Particle number concentrations for different size ranges
178 were then calculated from the SMPS measurements.

179 The 5-min PSD data were synchronized into hourly averages, and fitted by the
180 DO-FIT model developed by Hussein et al. (2005) according to the multiple
181 log-normal distribution algorithms. Based on the fitted PSD data, the PNCs were
182 classified into $4 \leq d \leq 25$ nm (N₄₋₂₅), $25 < d \leq 100$ nm (N₂₅₋₁₀₀), $4 \leq d \leq 100$ nm
183 (N₄₋₁₀₀), $100 < d \leq 736$ nm (N₁₀₀₋₇₃₆) and $4 \leq d \leq 736$ nm (N₄₋₇₃₆), for nucleation mode,
184 Aitken mode, ultrafine, accumulation mode and total particles, respectively. Pearson
185 correlation coefficient, r , was calculated by *PASW Statistics ver. 18* (SPSS Inc.) to
186 determine the correlation between the respective parameters.

187

188 **2.3 Classification of new particle formation and calculation of the particle growth 189 and formation rates**

190 A NPF event is defined as the increase of the number concentration of nucleation
191 mode particles, where those particles are growing into Aitken and/or accumulation
192 mode size range (≥ 25 nm) and last for a few hours until they coagulate on the
193 pre-existing aerosol and/or other surfaces in the atmosphere. The calculation of
194 particle growth rate (GR) was represented by the rate of geometric median diameter
195 changes during the period of nucleation mode particles growing through 25 nm
196 (Cheung et al., 2013). The formation rate (J) of nucleation mode particles for each
197 NPF event was calculated for the particle size ranging from 4-25 nm according to the
198 method of Dal Maso et al. (2005). The formation rate is defined as the sum of the
199 apparent formation rate (dN_{4-25}/dt) and the coagulation loss rate during the NPF event.
200 It should be noted that the reported apparent particle formation rate is expected to be
201 smaller than the actual nucleation rate, since some fraction of formed nuclei are

202 always scavenged by coagulation into larger pre-existing particles before they grow
203 larger by condensation (Lehtinen et al., 2007). The work done by Kulmala et al. (2012)
204 was referred for overview of the methodology on the measurement of the nucleation
205 of atmospheric particles.

206

207 ***2.4 Back-trajectory analysis***

208 Backward trajectories were calculated using the HYSPLIT model (Hybrid Single
209 Particle Lagrangian Integrated Trajectory, Version 4.9) of NOAA (National Oceanic
210 and Atmospheric Administration) (Draxler, 1999) for TARO during the sampling
211 period, in order to trace the origins of the air masses. 72-h back trajectories were
212 calculated twice per day at 00:00LT and 12:00LT with height setting of 200 m above
213 ground level. It should be noted that the grid resolution of the meteorological data
214 used for back-trajectories calculation is $1^\circ \times 1^\circ$, which is not enough to trace the
215 detailed air mass passage over the scale of the study region and, therefore, the
216 trajectories only provide an indication of the region from which the air mass was
217 originated.

218

219 ***3. Results and discussions***

220 ***3.1 Particle number concentration and size distribution in respective seasons***

221 As mentioned above, the air quality of urban Taipei is significantly affected by
222 both the local vehicular exhausts and long-range transport of air pollutants, where the
223 later is dominated by meteorological factors. The information on the meteorological
224 conditions, particularly the wind pattern, is important to elucidate our results and thus
225 presented here. The back-trajectories of the air masses for the TARO are illustrated in
226 **Figure 1 (left panel)**. The results showed that northeasterly winds prevailed in
227 autumn and winter seasons, passing through the Asian continent before reaching
228 Taiwan, whereas southerly winds prevailed in summertime. The air masses observed
229 in spring period were found to be mainly associated with Asian continental outflows
230 and occasionally with the southerly flows. This observation agreed with the surface
231 wind direction measured in urban Taipei area (see **Figure 1, right panel**), where
232 northeasterly winds were dominating during the period from November 2012 to May
233 2013, and southerly winds were prevailing from May 2013 to August 2013.

234

235 The particle number concentrations in various size ranges during each season are
236 summarized in **Table 1**. Relatively higher total PNCs (N_{4-736}) were observed in spring
237 and winter with median values of 19.4×10^3 and $17.4 \times 10^3 \text{ cm}^{-3}$, respectively, followed
238 by that of summer ($16.6 \times 10^3 \text{ cm}^{-3}$) and autumn ($13.9 \times 10^3 \text{ cm}^{-3}$). This result is
239 comparable to the previous measurements conducted in urban Taipei where the

240 seasonal means of PNCs ($10 < d < 560\text{nm}$) ranged from 11.0×10^3 to $17.0 \times 10^3 \text{ cm}^{-3}$
241 (Cheng et al. 2014). **Figure 2** illustrates the number, surface and volume size
242 distributions of the aerosol particles. The geometric mean diameter (GMD) of each
243 PSD mode was retrieved from the data of number concentration. The GMDs of the
244 nucleation, Aitken and accumulation modes were found to be 10.4-12.8 nm, 26.5-38.4
245 nm, and 91.8-159.0 nm, respectively. Details of particle number concentration and
246 GMDs of each fitted mode in four seasons were listed in **Table S1** of appendix.

247

248 In addition, the fitted GMDs of surface distribution were found to be 77.4 and
249 293 nm for autumn, 22.1, 68.9 and 228 nm for winter, 77.4 and 253 nm for spring,
250 and 12.9 and 268 nm for summer, respectively (not shown in the figures). In winter
251 and summer seasons, one of the fitted surface GMDs was located at nucleation mode,
252 showing the significant contribution of nucleation mode particles in these two seasons.
253 Bimodal volume distribution was obtained for all seasons where the fitted volume
254 GMDs were 96.3 and 372 nm for autumn, 71.8 and 275 nm for winter, 99.5 and 339
255 nm for spring, and 99.5 and 237 nm for summer, respectively. The GMD of first
256 volume mode was relatively stable in each season (i.e. 71.8-99.5 nm), but smaller
257 GMD (237 nm) for the second volume mode was observed in summer. The results
258 implied that a higher fraction of particles could have evolved from smaller size range
259 (i.e. nucleation and Aitken modes) into accumulation mode, which coincided with our
260 observation that NPF events occurred mostly in summer (see Section 3.4).
261 Furthermore, this seasonal variability agrees with our previous findings that the
262 growth rate of newly formed particles was correlated with the photolysis of ozone, an
263 indicator of photochemical activity (Cheung et al., 2013). The causes responsible for
264 the observed seasonal variations in PNCs will be detailed in the following sections.
265 This was different from that observed in urban Beijing where relatively larger GMD
266 was observed in accumulation mode due to the enhancement of condensation by
267 higher photochemical activities in summer but without significant seasonal variations
268 in Aitken mode distribution (Wu et al., 2008).

269

270 It was revealed that the nucleation mode particles were predominant in the PNCs
271 during autumn, winter and spring in the study area, whereas a distinct size distribution
272 pattern was observed in summertime. In summer, the fraction of nucleation ($N_{4-25} /$
273 N_{4-736}) decreased to 0.44 (see **Table 1**) and the Aitken mode PNCs increased to be
274 comparable to that of the nucleation mode, whereas the N_{4-25} / N_{4-736} ratios for other
275 seasons ranged from 0.56 to 0.77 (see **Table 1**). Observation from another aspect is
276 that the PNC of nucleation mode (N_{4-25}) peaked in winter and reached the minimum in
277 summer, whereas the PNCs of Aitken mode (N_{25-100}) and accumulation mode ($N_{100-736}$)

278 reached their maxima in summertime. The changes in the size distribution in summer
279 season were most likely due to the seasonally enhanced photochemical production of
280 condensable vapors that, in turn, contributed to the growth of aerosol particles in the
281 atmosphere.

282

283 **3.2 Mass concentration and chemical composition**

284 **Figures 3a** and **3b** illustrate the averaged chemical composition and mass
285 concentration of UFPs and PM₁, respectively, for each season. Details of the mass
286 concentration and chemical composition of UFPs and PM₁ are listed in Table S2 in
287 the appendix.

288

289 The seasonal means of UFPs ranged from 0.73 to 1.64 $\mu\text{g m}^{-3}$, with an annual
290 average of 1.01 $\mu\text{g m}^{-3}$. The measured UFPs mass concentration of the present study
291 was comparable to that in urban area of Los Angeles, United States (0.80 – 1.58 $\mu\text{g m}^{-3}$,
292 Hughes et al. 1998), and relatively higher than that in urban Helsinki, Finland
293 (average: 0.49 $\mu\text{g m}^{-3}$, Pakkanen et al. 2001). For the chemical composition, OC was
294 found to be the major mass contributor, which accounted for 29.8 % (seasonal means
295 ranging from 26.9 to 33.4 % for various seasons) of averaged mass concentration of
296 UFPs. The EC was the second major component with averaged mass contribution of
297 5.1 % (seasonal means: 2.4–7.6 %), followed by sulfate (SO_4^{2-}) at 4.3 % (seasonal
298 means: 3.4-6.4%) and nitrite (NO_2^-) at 2.9% (seasonal means: 0.9-7.3%). In addition,
299 a large fraction of mass was contributed by the group of “others”, which consisted of
300 mineral (K^+ , Ca^{2+} , PO_4^{3-} and Mg^{2+}), sea-salt (Na^+ and Cl^-), and unidentified species.
301 The results showed that, on average, mineral and sea salt components attributed only
302 3.5 % (seasonal means: 2.0-6.0 %) to UFPs mass concentration. Thus a substantial
303 amount of UFPs remained unidentified, which likely included hydrogen and oxygen
304 associated with OC. The conversion factors used to estimate the average molecular
305 weight per carbon in particulate organic matter varied depending on the characteristic
306 of aerosols. A lower factor value, 1.2, was usually suggested for saturated organic
307 molecules, while a higher value, 1.6, was adopted for water-soluble compounds
308 consisting of multifunctional oxygenated groups, and even higher factor values were
309 suggested for aged aerosols which contained higher portion of low and semi-volatile
310 products of photochemical reactions (Turpin and Lim et al. 2001). The high
311 un-identified mass fraction implied that the photochemical production of secondary
312 organic aerosols was a significant process responsible for the elevated UFPs levels
313 observed in this study.

314

315 As shown in Fig. 3b, average PM₁ was estimated to be 14.7 $\mu\text{g m}^{-3}$ (seasonal

316 means: 11.6-18.5 $\mu\text{g m}^{-3}$) in this study, which is similar to the results of a previous
317 study in urban Taipei (average: 14.0 $\mu\text{g m}^{-3}$, Li et al., 2010). The measured PM_{10} level
318 is relatively higher than that of the urban areas of Phoenix, United States (5.9 $\mu\text{g m}^{-3}$,
319 Lundgren et al. 1996) and Helsinki, Finland (6.1 $\mu\text{g m}^{-3}$, Vallius et al. 2000). For
320 chemical composition, sulfate was the major mass contributor of PM_{10} (average: 39.0
321 %, seasonal means: 33.8 - 46.8 %), followed by ammonium (average: 12.7 %, seasonal
322 means: 12.0 - 13.2 %) and OC (average: 11.5 %, seasonal means: 9.2 to 14.3
323 %).

324

325 The results presented above indicated that UFPs exhibited a distinct seasonal
326 variability and composition from PM_{10} in the study area. The highest UFPs
327 concentration was observed in summer (1.64 $\mu\text{g m}^{-3}$) and the lowest in winter (0.73
328 $\mu\text{g m}^{-3}$). This result may be attributed to the stronger photochemical activities in
329 summer which could have enhanced the formation of secondary organic aerosols.
330 Consequently, the mass concentration of OC increased from 0.20 $\mu\text{g m}^{-3}$ in winter to
331 0.47 $\mu\text{g m}^{-3}$ in summertime. It is noteworthy that the mass concentration of sulfate in
332 UFPs also peaked in summer (64 ng m^{-3}), suggesting enhancement in photo-oxidation
333 of SO_2 . Cheung et al. (2013) found that photo-oxidation of SO_2 was the major
334 mechanism for the formation of new particles in Taipei, Taiwan and the production of
335 condensable vapors was also dominated by photo-oxidation. The co-variations in
336 sulfate and OC revealed in this study further suggested that secondary organic
337 compounds were the major condensable matter contributing to the growth of newly
338 formed particles.

339

340 While the organics predominated in the mass concentration of UFPs, which
341 included nucleation mode and Aitken mode particles, the measurements of PM_{10} in this
342 study suggested that sulfate was the major constituent of accumulation mode aerosols.
343 In contrast to the seasonal variation of UFPs, the mass concentration of PM_{10} reached
344 the maximum at 18.5 $\mu\text{g m}^{-3}$ in spring and exhibited the minimum at 11.6 $\mu\text{g m}^{-3}$ in
345 summer. The PM_{10} differences between spring and summer were mostly due to
346 declined ambient levels of sulfate, nitrate, and ammonium ions. As a result, the mass
347 contribution of the three inorganic ions in PM_{10} reduced from 55.7 % to 46.2 % and,
348 on the contrary, the mass fraction of OC increased from 10.2 to 14.3 %. The seasonal
349 characteristics of PM_{10} concentration and composition were attributed mostly to the
350 changes in the origin areas of background air mass, which shifted from the Asia
351 Continent to the western Pacific Ocean during summertime (see **Fig. 1**). Our previous
352 studies reported that the fine particulate matter ($\text{PM}_{2.5}$) transported on the Asian
353 outflows to northern Taiwan maximized in springtime and were enriched in sulfate,

354 nitrate, and ammonium (Chou et al., 2008; 2010). The seasonal variability of PM_{10}
355 found in this study was consistent with the previous observations for $PM_{2.5}$ and
356 thereby suggested the significance of Asian outflow aerosols to the PM_{10} budget in the
357 downwind areas of the Asia Continent.

358

359 *3.3 Seasonal characteristics of photochemical production*

360 In order to study the influences of photochemical production of particles, the
361 measurements of PNC and PSD were analyzed per daytime (07:00 – 17:00 LT) and
362 nighttime (17:00 – 07:00 LT), respectively (see **Figure 4**). In urban environment, the
363 possible sources influencing the PNC and PSD are complicated, which include not
364 only the direct emission from primary sources but also interaction between the newly
365 formed particles, pre-existing particles and condensing vapors through the
366 condensation and coagulation processes. Nevertheless, these processes occurred
367 throughout the day and will not dominate in the differences between daytime and
368 nighttime PNCs as observed in this study. It was assumed that photochemical reaction
369 was the major attributing factor to the observed diurnal differences in PNC. Since the
370 particles in nighttime were mainly emitted from the vehicular exhausts and the
371 elevated PNCs in daytime were due to both the primary and secondary sources of the
372 particles in the study area (Cheung et al., 2013), a larger difference between the PNCs
373 observed in daytime and nighttime indicated stronger influences of photochemical
374 production on the PNCs. The most striking seasonal features shown in **Figure 4** is the
375 large difference between daytime against nighttime PSD in summer as indicated by
376 the low N_{4-736} (nighttime)/ N_{4-736} (daytime) ratio, whereas higher ratios were observed
377 in other seasons. In addition, the diurnal variation of particle size distribution (see
378 **Figure 5**) provided further information about the variations in PSD. Two nucleation
379 bursts were distinctly observed in morning and afternoon traffic peak hours in autumn,
380 winter, and spring, while a typical PSD pattern of nucleation event (increase of
381 nucleation mode particle concentrations with subsequent growth in particle size) was
382 dominant in summer. This result is as expected because the photochemical production
383 of nucleation mode particles is more intense during warm seasons (Cheung et al.,
384 2011). Moreover, as discussed in previous section, the photochemical reactions could
385 produce condensable organics that allows the newly formed nucleation mode particles
386 to grow into the Aitken mode. The relatively small differences between the daytime
387 and nighttime N_{4-736} in autumn and winter indicated that the photochemical
388 contribution in PNCs was declined as compared to that in summertime. Nevertheless,
389 the contribution of vehicle emission was also significant, especially during colder
390 seasons and when photochemical reactions were less intense. This will be discussed in
391 detail in Section 3.5.

392 3.4 Factors affecting new particle formation (NPF)

393 As shown in previous study, the NPF events were frequently observed in summer,
394 which subsequently induced a notable increase in N_{4-25} in urban Taipei (Cheung et al.
395 2013). The frequency of NPF events was found to be 10 out of 84 measurement days
396 and the events were observed in autumn (1 out of 23 days), spring (3 out of 26 days) and
397 summer (6 out of 14 days) seasons. **Figure 6** (a-d) shows the scatter plots of N_{4-25}
398 against NO_x for daytimes in each season. During the NPF events, a non-linear
399 relationship between these two parameters was usually observed during the daytime
400 (Cheung et al. 2013). The results showed that clear NPF events were observed often
401 in summer and occasionally in spring, but rarely in autumn and winter in the study
402 area. The averaged particle growth and formation rates were found to be $4.0 \pm 1.1 \text{ nm}$
403 h^{-1} and $1.4 \pm 0.8 \text{ cm}^{-3} \text{ s}^{-1}$, which were comparable to those measured in other urban
404 studies in Asian cities such as Hong Kong (average: 6.7 nm h^{-1} , Wang et al., 2014)
405 and Beijing (average: 5.2 nm h^{-1} , Wang et al., 2013), and also within the range
406 observed in other nucleation studies across the globe ($\sim 1 - 20 \text{ nm h}^{-1}$, Kulmala et al.,
407 2004). The particle growth and formation rates of each case are listed in **Table 2**.

408

409 **Table 3** summarizes the averages of N_{4-25} , PM_{10} , H_2SO_4 proxy (as
410 $\text{UVB} \cdot \text{SO}_2 / \text{condensation sink}$) and wind speed for each season. Petäjä et al. (2009)
411 calculated the H_2SO_4 proxy with a pre-factor value, k , and use it to estimate the actual
412 sulfuric acid concentration. The estimation of a site-specific k value requires an actual
413 measurement of H_2SO_4 which is not available in this study area. The proxy value
414 calculated in this study was therefore only used as an indicator of particle production
415 strength contributed by H_2SO_4 . The dominating factors associated to the frequent
416 particle formation in summertime were the low PM_{10} concentration ($35.6 \mu\text{g m}^{-3}$) and
417 high H_2SO_4 proxy ($493.1 \text{ ppb W m}^{-2} \text{ s}$). The association of sulfuric acid production
418 and the NPF events agreed with the elevated mass concentration of sulfate in UFPs
419 during summertime (shown in **Table S2**), as well as the results of previous urban
420 studies (Woo et al. 2001; Cheung et al. 2013). This strongly suggested that the new
421 particle formation was mainly driven by the photochemical oxidation of SO_2 under
422 low condensation sink conditions (Gao et al., 2009; Nie et al., 2014), where the SO_2
423 could be transported from the upwind area on the summer monsoons (see **Figure 1d**).
424 Contrarily, the absence of particle formation events in wintertime could be attributed
425 to the declined photochemical production of H_2SO_4 as well as suppression of NPF by
426 particles transported from the Asian continent (Lin et al., 2004). The results of this
427 work evidenced that low PM_{10} concentration and high sulfuric acid production
428 favored the particle formation process in urban areas. Nevertheless, it should be noted
429 that condensing vapors other than sulfuric acid, for example VOCs, could also

430 contribute to the observed particle formation, which requires further investigation.

431

432 The scatter plot between UVB*SO₂ and condensation sink is depicted in **Figure**
433 **7**. Relatively higher UVB*SO₂ values were obtained during NPF events. Notably,
434 there was a group of data with high UVB*SO₂/CS but low UVB*SO₂ where no NPF
435 event was observed. This implied that there could be a threshold level of UVB*SO₂
436 for NPF in the study region. However, some exceptions existed in the dataset and
437 suggested that the parameters driving NPF have not been well accounted and need to
438 be further studied. It was also noticed that an Asian outflow event occurred on 7 April
439 2013 during which an atypical NPF was observed (labeled as black dot in **Figure 7**).
440 This could be relevant to the secondary particle formation on dust surface under the
441 influence of long-range transport of air mass. This will be discussed in further details
442 in Section 3.6.

443

444 **3.5 Influences of local emission on PNCs**

445 Vehicle emission is known as the major source of the particulate matter in urban
446 environment, particularly during the nighttime. In order to investigate the relationship
447 between the vehicular exhausts and PNCs, the scatter plots of NO_x (as an indicator of
448 vehicle emission) against N₄₋₂₅, N₂₅₋₁₀₀ and N₁₀₀₋₇₃₆ during the nighttime were
449 examined for winter and summer periods (see **Figure 8**). The values of the Pearson
450 correlation coefficient (r) and the slope of linear regression between NO_x and PNCs
451 are summarized in **Table 4**.

452

453 The highest r values were found in both the plots of NO_x against N₂₅₋₁₀₀ for
454 winter ($r = 0.88$) and summer ($r = 0.87$). This result suggested a strong linear
455 correlation between the vehicle emission and the N₂₅₋₁₀₀ which coincided with the
456 results from previous studies (e.g., Morawska et al. 2008). During wintertime,
457 stronger correlation was found between NO_x against N₄₋₂₅ ($r = 0.84$) and N₂₅₋₁₀₀ ($r =$
458 0.88) compared to that between NO_x and N₁₀₀₋₇₃₆ ($r = 0.38$). In contrast, high r values
459 were obtained between NO_x and all particle modes in summer ($r = 0.70 - 0.87$). The
460 robust correlation of NO_x and N₄₋₂₅, also NO_x and N₂₅₋₁₀₀ suggested that local vehicle
461 emission was the predominant source of UFPs throughout a year. These results
462 coincided with previous studies on the size distribution of vehicle exhaust particles,
463 which were found to be 20-130 nm and 20-60 nm, respectively, for diesel and petrol
464 engine vehicles (Harris and Maricq 2001, Ristovski et al. 2006). However, the PNCs
465 of accumulation mode particles (N₁₀₀₋₇₃₆) in winter were dominated by
466 NO_x-independent sources, which were most likely related to the pollution outbreaks
467 from the Asian continent. Lin et al. (2004) indicated that the long-range transported
468 air mass was characterized by high level of PM₁₀ and low mixing ratio of NO_x due to

469 its short atmospheric lifetime. Interestingly, a moderate correlation between the PNC
470 of accumulation mode particles ($N_{100-736}$) and NO_x was also observed in summer.
471 Given that the Asian outflow was ceased in summertime, this correlation evidenced
472 substantial contribution of local sources, particularly vehicular emissions, to the PNC
473 of accumulation mode particles in Taipei, Taiwan.

474

475 The slope values can serve as a relative emission factor of particles per NO_x ,
476 which indicates the degree of influence of vehicle emission on the PNCs (Cheung et
477 al., 2013). The corresponding slope values for N_{4-25} , N_{25-100} , and $N_{100-736}$, were found
478 to be 279, 163, 18 $cm^{-3} \cdot ppb^{-1}$ in winter, and 239, 330, 155 $cm^{-3} \cdot ppb^{-1}$ in summer.
479 Larger sum of slope values (724 vs. 460 $cm^{-3} \cdot ppb^{-1}$) was found in summertime
480 compared to winter period, evidencing a greater influence of the vehicle emission on
481 particle number concentration. The seasonal effects on the emission ratio of PNCs and
482 NO_x are rather difficult to address due to the complexity of different controlling
483 factors, such as formation mechanisms and meteorological conditions. For example,
484 Nam et al. (2010) reported negatively exponential correlation between the PM/NO_x
485 ratio in vehicle emission and ambient temperature, and suggested that the impact of
486 ambient temperature on particulate matter was larger than that on NO_x . Nevertheless,
487 the observed differences in the PNCs/ NO_x ratios for winter and summer periods of
488 this study necessitate further investigations on the formation mechanisms of aerosol
489 particles in urban areas, in particular the nucleation and the Aitken modes.

490

491 **3.6 Influence of long-range transport (LRT)**

492 During the seasons of winter monsoons, i.e. from autumn to spring, the
493 continental outflows have been frequently observed in urban Taipei, which is
494 indicated by the stable northeasterly wind and increase of O_3 level (Lin et al. 2004).
495 Previous studies of long-range transport (LRT) of air pollutants on air quality of
496 northern Taiwan showed that an elevated PM_{10} was observed under the influence of
497 continental outflows (Lin et al., 2004, Chou et al., 2004). **Figure 9** depicts an LRT
498 pollution event observed at the TARO during this study. The wind direction changed
499 from westerly/northwesterly to northeasterly at 21:00, 24 March which continued
500 until 06:00, 26 March. During this period, the O_3 mixing ratio remained at moderate
501 level (~30-55 ppb) and PM_{10} increased from 10.0 to 98.0 $\mu g m^{-3}$. It should be noted
502 that the variations of measured pollutants were not solely influenced by the
503 long-range transport, but also partly due to the variation of local pollution and
504 boundary dynamics. In this section, we attempt to analyze the PSD/PNC under the
505 influences of continental pollution outbreaks. The periods of the respective LRT
506 events are listed in **Table S3**.

507

508 As shown in **Figure 9**, the diurnal variations of PSD during the LRT event
509 exhibited two N_{4-25} peaks associated to the morning and afternoon traffic rush hours,
510 whereas the PNCs of the Aitken mode particles remained at a low level. The results
511 suggested that the influences of local vehicle emission on PNCs were still in place,
512 whereas growth of particles due to secondary production of condensable vapors could
513 have been suppressed, as NPF was rarely observed during the LRT events. It is
514 noteworthy that a weak dust transport event was observed on 7 April 2013 where a
515 nucleation event was observed in the PSD, evidencing that secondary formation of
516 particles could have had occurred. However, the dominating diameter of particles was
517 ~ 40 -50 nm at the initial stage of the event. The nucleation event initiated since
518 $\sim 06:00$ LT until $21:00$ LT, when the northeasterly wind prevailed. The PM_{10} and O_3
519 increased from minima of $44 \mu\text{g m}^{-3}$ (at $06:00$ LT) and 25 ppb (at $05:00$ LT) to the
520 daily maxima of $92 \mu\text{g m}^{-3}$ (at $17:00$ LT) and 61 ppb (at $16:00$ LT). This result showed
521 that the NPF process could have occurred in the upwind area where newly formed
522 particles were transported to the study site, or heterogeneously formed particles were
523 released from the dust surface during the long-range transport of air pollutants (Nie et
524 al., 2014).

525

526 The averaged PSDs for LRT and non-LRT cases are shown in Figure 10. The
527 GMDs of the nucleation, Aitken, and accumulation modes in PSD were found to be
528 10.4, 37.2 and 158 nm for LRT and 11.4, 30.4 and 114 nm for non-LRT cases,
529 respectively (see Table S1 for detailed fit results of the PSD for LRT and non-LRT
530 cases). The PNCs of different modes observed in non-LRT events were $8.6 \times 10^3 \text{ cm}^{-3}$
531 (nucleation mode), $9.3 \times 10^3 \text{ cm}^{-3}$ (Aitken mode) and $2.6 \times 10^3 \text{ cm}^{-3}$ (accumulation
532 mode). The PNCs of LRT events were $9.2 \times 10^3 \text{ cm}^{-3}$ (nucleation mode), $4.0 \times 10^3 \text{ cm}^{-3}$
533 (Aitken mode), and $1.3 \times 10^3 \text{ cm}^{-3}$ (accumulation mode), respectively. The nucleation
534 mode PNC observed in non-LRT was comparable with that in LRT events, whereas
535 significant higher PNCs for the Aitken mode and accumulation mode were observed
536 during non-LRT periods. This was attributed to the lower average wind speed (and
537 hence poor dispersion) during non-LRT events ($1.5 \pm 0.8 \text{ m s}^{-1}$) than that for LRT
538 events ($3.0 \pm 0.8 \text{ m s}^{-1}$). In contrast to the increase in PM_{10} observed usually during
539 LRT episodes (e.g., Lin et al., 2012), the relatively lower PNCs suggested that the
540 number concentration of submicron particles, in particular UFPs, was dominated by
541 local emissions. This agreed with the observation of seasonal UFPs mass
542 concentration that peaked in summertime when Taiwan was isolated from the
543 influences of continental air mass.

544

545 **4. Conclusions**

546 The mass concentration and chemical composition of ultrafine particles (UFPs)
547 and submicron particles (i.e. PM₁) as well as the particle number concentration (PNC)
548 and size distributions (PSD) with size ranging from 4 to 736 nm were measured
549 during four seasonal campaigns in the period from October 2012 to August 2013 at
550 the TARO, a subtropical urban aerosol station in Taipei, Taiwan. Distinct seasonal
551 variability and chemical composition of UFPs and PM₁ were revealed. The UFPs
552 were composed mostly of organic matter and reached maxima in summer, whereas the
553 PM₁ composition was dominated by ammonium and sulfate and exhibited a seasonal
554 peak in spring.

555

556 It was found that the total PNC was significantly elevated during cold seasons,
557 which was caused mostly by the high level of nucleation mode particles (N₄₋₂₅). On
558 the contrary, both the Aitken mode (N₂₅₋₁₀₀) and accumulation mode (N₁₀₀₋₇₃₆) PNCs
559 reached their respective maxima in summertime. Consistent correlation without
560 significant seasonal variations was found between the UFPs (i.e. nucleation and
561 Aitken mode particles) and NO_x, suggesting that local vehicle emission was the major
562 source of UFPs in the study area throughout a year. The local vehicle emission was
563 also dominating the accumulation mode PNC in summer, but not in wintertime. The
564 declined correlation between NO_x and N₁₀₀₋₇₃₆ in winter was likely due to the
565 influences of air pollution associated with the Asian outflows.

566

567 The elevated UFPs level in summer was attributed to the increase in the
568 concentration of Aitken mode particles (N₂₅₋₁₀₀). It was revealed from the
569 measurements of PSD that a large number of nucleation mode particles could have
570 evolved into the Aitken mode during summertime, which was most likely relevant to
571 the photochemical production of condensable vapors that, in turn, could have
572 contributed to the growth of particles in the atmosphere. Moreover, the chemical
573 measurements suggested that the constituents of the condensed materials in UFPs
574 were mostly organic matter, implying the significance of secondary organic aerosols
575 in the ambient UFPs.

576

577 A total of 10 new particle formation (NPF) events occurred out of 84
578 measurement days in this study, which were observed in autumn (1 out of 23 days),
579 spring (3 out of 26 days) and summer (6 out of 14 days) seasons. The prevalence of
580 NPF in summer agreed with the highest H₂SO₄ proxy and lowest PM₁₀ observed in
581 this study, which provided favorable atmospheric conditions for new particle
582 formation. The averaged particle growth and formation rates for the NPF events were

583 $4.0 \pm 1.1 \text{ nm h}^{-1}$ and $1.4 \pm 0.8 \text{ cm}^{-3} \text{ s}^{-1}$, respectively, which were comparable to those
584 measured in previous urban studies.

585

586 As exemplifying above, the characteristics of various physicochemical properties
587 of particles investigated in this study and the occurrence of NPF exhibited a strong
588 seasonal variability, which was co-influenced by the long-range transported particles
589 during the seasons of winter monsoons and the strong photochemical activities in
590 summer. The results of this study are critical for the authorities involved in urban
591 development and health impact assessment, and the environmental policy makers who
592 are tackling the severe atmospheric pollution in the East Asia region.

593

594 *Acknowledgements*

595 This research was supported by the Academia Sinica and the Ministry of Science and
596 Technology of Taiwan through grants 103-2111-M-001-003, 102-2628-M-001-007,
597 and 101-2119-M-001-003. The authors thank the Taiwan EPA for providing the air
598 quality and meteorological data. We also thank the Department of Atmospheric
599 Science of National Taiwan University for the logistical supports to the operation of
600 TARO. Prof. Tareq Hussein is gratefully acknowledged for providing us the code of
601 DO-FIT.

602

603 **Table 1.** Median and quartile ranges (Q1-Q3) of the PNCs measured in each season. The size
604 ranges of the PNCs were represented by the subscripted number. For example, N_{4-25} ,
605 represents the number concentrations of the particles from 4 to 25 nm. The fractions of N_{4-25}
606 and N_{4-100} to total PNCs were presented in the last two columns.

607

	<i>Measurement periods</i>	N_{4-736} (10^3 \#/cm^3)	N_{4-25} (10^3 \#/cm^3)	N_{25-100} (10^3 \#/cm^3)	N_{4-100} (10^3 \#/cm^3)	$N_{100-736}$ (10^3 \#/cm^3)	N_{4-25}/N_{4-736}	N_{4-100}/N_{4-736}
<i>Autumn</i>	24 Oct–15 Nov 2012	13.9 (9.9–19.4)	8.6 (5.8– 11.8)	3.9 (2.6–5.5)	12.7 (8.7–17.8)	1.3 (0.8–1.9)	0.62	0.90
<i>Winter</i>	4–24 Jan 2013	17.4 (12.7–22.3)	11.6 (8.2–15.1)	4.1 (2.8–5.6)	16.3 (11.6–21.4)	0.9 (0.5–1.5)	0.70	0.94
<i>Spring</i>	17 Mar–11 Apr 2013	19.4 (13.2–26.2)	10.3 (7.2–14.1)	5.8 (4.0–9.4)	17.0 (11.4–23.6)	1.9 (1.4–2.7)	0.56	0.89
<i>Summer</i>	1–14 Aug 2013	16.6 (9.2–26.7)	6.9 (4.5–10.4)	6.0 (2.5–11.3)	13.7 (7.9–21.4)	3.1 (0.5–5.1)	0.44	0.87

608

609 **Table 2.** Time periods defined as the new particle formation events and the particle growth
 610 and formation rates

<i>Date</i>	<i>Time period (LT)</i>	<i>Growth rate (nm h⁻¹)</i>	<i>Formation rate (cm⁻³ s⁻¹)</i>
9 Nov 2012	07:00-13:00	3.4	1.30
26 Mar 2013	06:00-10:00	3.4	1.91
4 Apr 2013	07:00 – 10:00	3.7	1.13
5 Apr 2013	08:00 – 12:00	5.5	1.10
4 Aug 2013	09:00 – 12:00	3.9	1.84
5 Aug 2013	09:00 – 13:00	4.9	2.44
7 Aug 2013	06:00 – 12:00	3.5	0.84
8 Aug 2013	09:00 – 12:00	5.0	2.76
9 Aug 2013	06:00 – 13:00	1.6	0.39
11 Aug 2013	06:00 – 09:00	4.8	0.58
Average (±Standard Deviation)		4.0 (±1.1)	1.4 (±0.8)

611

612

613 **Table 3.** Average of N_{4-25} , PM_{10} , UVB, SO_2 , condensation sink (CS), H_2SO_4 proxy and wind
614 speed of different seasons. Standard deviation values shown in brackets (Note: the data with
615 observation of rainfall was not used in calculation).

<i>Periods</i>	<i>N_{4-25}</i> (10^3 \#/cm^3)	<i>PM_{10}</i> ($\mu\text{g m}^{-3}$)	<i>UVB</i> (Wm^{-2})	<i>SO_2</i> (ppb)	<i>CS</i> ($10^{-2} s^{-1}$)	<i>H_2SO_4 proxy</i> (ppb $Wm^{-2} s$)	<i>Wind speed</i> (ms^{-1})
Autumn	8.6 (± 4.5)	53.9 (± 21.4)	1.04 (± 1.75)	2.27 (± 1.44)	0.8 (± 0.5)	307.1 (± 609.1)	2.8 (± 1.0)
Winter	11.6 (± 9.2)	48.4 (± 23.9)	0.80 (± 1.47)	2.58 (± 1.61)	0.8 (± 0.6)	240.0 (± 472.1)	2.3 (± 0.9)
Spring	10.2 (± 9.2)	61.1 (± 27.0)	0.99 (± 1.73)	2.76 (± 1.67)	1.4 (± 0.7)	238.4 (± 533.6)	2.2 (± 1.2)
Summer	6.9 (± 9.1)	35.6 (± 13.7)	1.97 (± 2.95)	3.19 (± 2.55)	1.9 (± 1.5)	493.1 (± 1066)	2.3 (± 1.1)

616

617 **Table 4.** Pearson correlation coefficient (r) and slope of linear regression of PNCs against
 618 NO_x during the nighttime (20:00-04:00 LT) in winter and summer periods.

<i>Periods</i>		N_{4-25}	N_{25-100}	$N_{100-736}$
Winter	<i>Slope</i>	279	163	18
	r	0.84	0.88	0.38
Summer	<i>Slope</i>	239	330	155
	r	0.76	0.87	0.70

619

620 **References**

- 621 Buzorius, G., McNaughton, C.S., Clarke, A.D., Covert, D.S., Blomquist, B., Nielsen,
622 K. and Brechtel, F.J. (2004). Secondary aerosol formation in continental outflow
623 conditions during ACE-Asia. *Journal of Geophysical Research*, 109,
624 doi:10.1029/2004JD004749.
- 625 Charlson, R.J., Schwartz, S.E., Hales, J.M., Cess, R.D., Coakley Jr., J.A., Hansen, J.E.
626 and Hofmann, D.J. (1992). Climate forcing by anthropogenic aerosols. *Science*, 255,
627 423-430.
- 628 Chen, S.-C., Hsu, S.-C., Tsai, C.-J., Chou, Charles, C.-K., Lin, N.-H., Lee, C.-T.,
629 Roam, G.-D., Pui, D.Y.H. (2013). Dynamic variations of ultrafine, fine and coarse
630 particles at the Lu-Lin background site in East Asia. *Atmospheric Environment*, 78,
631 154-162.
- 632 Cheng, Y.-H., Kao, Y.-Y. and Liu, J.-J. (2014). Correlations between black carbon
633 mass and size-resolved particle number concentrations in the Taipei urban area: A
634 five-year long-term observation. *Atmospheric Pollution Research*, 5, 62-72.
- 635 Cheung, H.C., Wang, T., Baumann, K. and Guo, H. (2005). Influence of regional
636 pollution outflow on the concentrations of fine particulate matter and visibility in the
637 coastal area of southern China. *Atmospheric Environment*, 39, 6463-6474.
- 638 Cheung, H.C., Morawska, L. and Ristovski, Z.D. (2011). Observation of new particle
639 formation in subtropical urban environment. *Atmospheric Chemistry and Physics*, 11,
640 3823-3833.
- 641 Cheung, H.C., Chou, C.C.-K., Huang, W.-R. and Tsai, C.-Y. (2013). Characterization
642 of ultrafine particle number concentration and new particle formation in an urban
643 environment of Taipei, Taiwan. *Atmospheric Chemistry and Physics*, 13, 8935-8946.
- 644 Chou, C. C.-K., Lee, C. T., Cheng, M. T., Yuan, C. S., Chen, S. J., Wu, Y. L., Hsu, W.
645 C., Lung, S. C., Hsu, S. C., Lin, C. Y., Liu, S. C. (2010). Seasonal variations and
646 spatial distribution of carbonaceous aerosols in Taiwan, *Atmos. Chem. Phys*, 10,
647 9563–9578.
- 648 Chou, C. C.-K., Lee, C.-T., Yuan, C. S., Hsu, W. C., Hsu, S. C., Liu, S. C. (2008).
649 Implications of the chemical transformation of Asian outflow aerosols for the
650 long-range transport of inorganic nitrogen species. *Atmospheric Environment*, 42,
651 7508-7519.
- 652 Chou, C. C.-K., Huang, S.-H., Chen, T.-K., Lin, C.-Y. and Wang, L.-C. (2005).
653 Size-segregated characterization of atmospheric aerosols in Taipei during Asian
654 outflow episodes. *Atmospheric Research*, 75, 89-109.
- 655 Chou, C. C.-K., Lin, C.-Y., Chen, T.-K., Hsu, S.-C., Lung, S.-C., Liu, S.C. and Young,
656 C.-Y. (2004). Influence of Long-Range Transport Dust Particles on Local Air
657 Quality: A Case Study on Asian Dust Episodes in Taipei during the Spring of 2002.

658 Terrestrial, Atmospheric and Oceanic Sciences, 15, 881-889.

659 Chow, J. C., Watson, J. G., Chen, L.-W. A., Chang, L.C.O., Robinson, N. F., Trimble,
660 D. and Kohl, S. (2007). The IMPROVE_A Temperature Protocol for
661 Thermal/Optical Carbon Analysis: Maintaining Consistency with a Long-Term
662 Database, *Journal of the Air & Waste Management Association*, 57:9, 1014-1023.

663 Dal Maso, M., Kulmala, M., Riipinen, I., Wagner, R., Hussein, T., Aalto, P.P. and
664 Lehtinen, K.E.J. (2005). Formation and growth of fresh atmospheric aerosols: eight
665 years of aerosol size distribution data from SMEAR II, Hyytiälä, Finland. *Boreal*
666 *Environ. Res.*, 10, 323-336.

667 Donaldson, K., Li, X.Y. and MacNee, W (1998). Ultrafine (nanometre) particle
668 mediated lung injury. *Journal of Aerosol Science*, 29, 553, 560.

669 Draxler, R.R. (1999). HYSPLIT4 user's guide. NOAA Tech. Memo. ERL ARL-230,
670 NOAA Air Resources Laboratory, Silver Spring, MD.

671 Gao, J., Wang, T., Zhou, X. Wu, W. and Wang, W. (2009). Measurement of aerosol
672 number size distributions in the Yangtze River delta in China: Formation and growth
673 of particles under polluted conditions. *Atmos. Environ.*, 43, 829-836.

674 Guo, H., Ding, A., Morawska, L., He, C., Ayoko, G., Li, Y. and Hung, W. (2008). Size
675 distribution and new particle formation in sub-tropical eastern Australia.
676 *Environmental Chemistry*, 5, 382-390.

677 Harris, S.J. and Maricq, M.M. (2001). Signature size distributions for diesel and
678 gasoline engine exhaust particulate matter. *Journal of Aerosol Science*, 32, 749-764.

679 Holman, J.P. (1972). *Heat Transfer*. New York, McGraw-Hill.

680 Holmes, N.S. (2007). A review of particle formation events and growth in the
681 atmosphere in the various environments and discussion of mechanistic implications.
682 *Atmospheric Environment*, 41, 2183-2201.

683 Hsu, S.-C., Lee, C.S.L., Huh, C.-A., Shaheen, R., Lin, F.-J. and Liu, S.C. (2014).
684 Ammonium Deficiency Caused by Heterogeneous Reactions during a Super Asian
685 Dust Episode. *Journal of Geophysical Research*, 119(11),
686 doi:10.1002/2013JD021096.

687 Hughes, L.S., Cass, G.R., Gonyea, J., Ames, M. and Olmez, I. (1998). Physical and
688 Chemical Characterization of Atmospheric Ultrafine Particles in the Los Angeles
689 Area. *Environmental Science and Technology*, 32, 1153-1161.

690 Hussein, T., Dal Maso, M., Petäjä, T., Koponen, I.K., Paatero, P., Aalto, P.P., Hämeri,
691 K. and Kulmala, M. (2005). Evaluation of an automatic algorithm for fitting the
692 particle number size distributions. *Boreal Env. Res.* 10:337-355.

693 Juwono, A., Johnson, G.R., Mazaheri, M. and Morawska, L., Roux, F. and Kitchen, B.
694 (2013). Investigation of the airborne submicrometer particles emitted by dredging
695 vessels using a plume capture method. *Atmospheric Environment*, 73, 112-123.

696 Kulmala, M. (2003). How Particles Nucleate and Grow. *Science*, 302, 1000-1001.

697 Kulmala, M., Kontkanen, J., Junninen, H., Lehtipalo, K., Manninen, H.E., Nieminen,
698 T., Petäjä, T., Sipilä, M., Schobesberger, S., Rantala, P., Franchin, A., Jokinen, T.,
699 Järvinen, E., Äijälä, M., Kangasluoma, J., Hakala, J., Aalto, P.P., Paasonen, P.,
700 Mikkilä, J., Vanhanen, J., Aalto, J., Hakola, H., Makkonen, U., Ruuskanen, T.,
701 Mauldin III, R.L., Duplissy, J., Vehkamäki, H., Bäck, J., Kortelainen, A., Riipinen I.,
702 Kurtén, T., Johnston, M.V., Smith, J.N., Ehn, M., Mentel, T.F., Lehtinen, K.E.J.,
703 Laaksonen, A., Kerminen, V.-M. and Worsnop, D.R. (2013). Direct Observations of
704 Atmospheric Aerosol Nucleation. *Science*, 339, 943-946.

705 Kulmala, M., Petäjä, T., Nieminen, T., Sipilä, M., Manninen, H.E., Lehtipalo, K., Dal
706 Maso, M., Aalto, P.P., Junninen, H., Paasonen, P., Riipinen, I., Lehtinen, K.E.,
707 Laaksonen, A. and Kerminen, V.-M. (2012). Measurement of the nucleation of
708 atmospheric aerosol particles. *Nature Protocols*, 7, 1651-1667.

709 Kulmala, M., Vehkamäki, H., Petäjä, T., Dal Maso, M., Lauri, A., Kerminen, V.-M.,
710 Birmili, W. and McMurry, P.H. (2004). Formation and growth rates of ultrafine
711 atmospheric particles: a review of observations. *Journal of Aerosol Science*, 35,
712 143-176.

713 Lehtinen, K.E.J., Dal Maso, M., Kulmala, M. and Kerminen, V.-M. (2007).
714 Estimating nucleation rates from apparent particle formation rates and vice versa:
715 Revised formulation of the Kerminen-Kulmala equation. *J. Aerosol Sci.*, 38,
716 988-994, doi:10.1016/j.jaerosci.2007.06.009.

717 Li, C.-S. and Lin, C.-H. (2010). PM1/PM2.5/PM10 Characteristics in the Urban
718 Atmosphere of Taipei. *Aerosol Science and Technology*, 36:4, 469-473.

719 Lin, C.-Y., Liu, S.C., Chou, C.C.-K., Liu, T.H. and Lee, C.-T. (2004). Long-Range
720 Transport of Asian Dust and Air Pollutants to Taiwan. *Terr. Atmos. and Ocean. Sci.*,
721 15, 759-784.

722 Lin, C.-Y., Chou, C. C.-K., Wang, Z., Lung, S.-C., Lee, C.-T., Yuan, C.-S., Chen,
723 W.-N., Chang, S.-Y., Hsu, S.-C., Chen, W.-C. and Liu, S. C. (2012). Impact of
724 different transport mechanisms of Asian dust and anthropogenic pollutants to Taiwan.
725 *Atmos. Environ.*, 60, 403-418.

726 Lundgren, D.A. Hlaing, D.N., Rich, T.A. and Marple, V.A. (1996). PM₁₀/PM_{2.5}/PM₁
727 Data from a Trichotomous Sampler. *Aerosol Science and Technology*, 25, 353-357.

728 Marple, V. A., Rubow, K. L. and Behm, S. M. (1991). A Microorifice Uniform
729 Deposit Impactor (MOUDI): Description, Calibration, and Use, *Aerosol Science and*
730 *Technology*, 14:4, 434-446.

731 Matsumoto, K., Uyama, Y., Hayano, T., Tanimoto, H., Uno, Itsushi. and Uematsu, M.
732 (2003). Chemical properties and outflow patterns of anthropogenic and dust
733 particles on Rishiri Island during the Asian Pacific Regional Aerosol

734 Characterization Experiment (ACE-Asia). *Journal of Geophysical Research*, 108
735 (D23), 8666, doi:10.1029/2003JD003426.

736 Mazaheri, M., Johnson, G.R. and Morawska, L. (2009). Particle and Gaseous
737 Emissions from Commercial Aircraft at Each Stage of the Landing and Takeoff
738 Cycle. *Environmental Science and Technology*, 43, 441-446.

739 Morawska, L., Ristovski, Z., Jayaratne, E.R., Keogh, D.U. and Ling, X. (2008).
740 Ambient nano and ultrafine particles from motor vehicle emissions: Characteristics,
741 ambient processing and implications on human exposure. *Atmospheric Environment*,
742 42, 8113-8138.

743 Nam, E., Kishan, S., Baldauf, R.W., Fulper, C.R., Sabisch, M. and Warila, J. (2010).
744 Temperature Effects on Particulate Matter Emissions from Light-Duty,
745 Gasonline-Powered Motor Vehicles. *Environmental Science and Technology*, 44,
746 4672-4677.

747 Nie, W., Ding, A., Wang, T., Kerminen, V.-M., George, C., Xue, L., Wang, W., Zhang,
748 Q., Petäjä, T., Qi, X., Gao, Xiaomei, Wang, X., Yang, X., Fu, C. and Kulmala.
749 (2014). Polluted dust promotes new particle formation and growth. *Scientific*
750 *Reports*, 4, 6634.

751 Pakkanen, T.A., Kerminen, V.-M., Korhonen, C.H., Hillamo, R.E., Aarnio, P.,
752 Koskentalo, T. and Maenhaut, W. (2001). Urban and rural ultrafine (PM_{0.1}) particles
753 in the Helsinki area. *Atmospheric Environment*, 35, 4593-4607.

754 Pérez, N., Pey, J., Cusack, M., Reche, C., Querol, X., Alastuey, A. and Viana, M
755 (2010). Variability of Particle Number, Black Carbon, and PM₁₀, PM_{2.5} and PM₁
756 Levels and Speciation: Influence of Road Traffic Emissions on Urban Air Quality.
757 *Aerosol Science and Technology*, 44, 487-499.

758 Petäjä, T., Mauldin III, R.L., Kosciuch, E., McGrath, J., Nieminen, T., Paasonen, P.,
759 Boy, M., Adamov, A., Kotiaho, T. and Kulmala, M. (2009). Sulfuric acid and OH
760 concentrations in a boreal forest site. *Atmospheric Chemistry and Physics*, 9,
761 7435-7448.

762 Pey, J., Rodríguez, S., Querol, X., Alastuey, A., Moreno, T., Putaud, J.P., and Van
763 Dingenen, R (2008). Variations of urban aerosols in the western Mediterranean.
764 *Atmospheric Environment*, 42, 9052-9062.

765 Pey, J., Querol, X., Alastuey, A., Rodriguez, S., Putaud, J.P. and Van Dingenen, R.
766 (2009). Source apportionment of urban fine and ultrafine particle number
767 concentration in a Western Mediterranean city. *Atmospheric Environment*, 43,
768 4407-4415.

769 Reche, C., Querol, X., Alastuey, A., Viana, M., Pey, J., Moreno, T., Rodríguez, S.,
770 González, Y., Fernández-Camacho, R., de la Rosa, J., Dall'Osto, M., Prévôt, A.S.H.,
771 Hueglin, C., Harrison, R.M. and Quincey, P. (2011). New considerations for PM,

772 Black Carbon and particle number concentration for air quality monitoring across
773 different European cities. *Atmospheric Chemistry and Physics*, 11, 6207-6227, 2011.

774 Ristovski, Z.D., Jayaratne, E.R., Lim, M., Ayoko, G.A. and Morawska, L. (2006).
775 Influence of diesel fuel sulphur on the nanoparticle emissions from city buses.
776 *Environmental Science and Technology*, 40, 1314-1320.

777 Salvador, C.M. and Chou, C.C.-K. (2014). Analysis of semi-volatile materials (SVM)
778 in fine particulate matter. *Atmospheric Environment*, 95, 288-295.

779 Subramanian, R., Khlystov, A.Y., Cabada, J.C. and Robinson, A.L. (2004). Positive
780 and negative artifacts in particulate organic carbon measurements with denuded and
781 undenuded sampler configurations. *Aerosol Science and Technology*, 38, 27-48.

782 Turpin, B.J. and Lim, H.-J. (2001). Species contributions to PM_{2.5} mass
783 concentrations: revisiting common assumptions for estimating organic mass. *Aerosol*
784 *Science and Technology*, 35, 602-610.

785 Vallius, M.J. Ruuskanen, J. Mirme, A. and Pekkanen, J. (2000). Concentrations and
786 Estimated Soot Content of PM₁, PM_{2.5} and PM₁₀ in a Subarctic Urban Atmosphere.
787 *Environmental Science and Technology*, 34, 1919-1925.

788 Wang, T., Ding, A.J., Blake, D.R., Zahorowski, W., Poon, C.N. and Li, Y-S. (2003).
789 Chemical characterization of the boundary layer outflow of air pollution to Hong
790 Kong during February-April 2001.

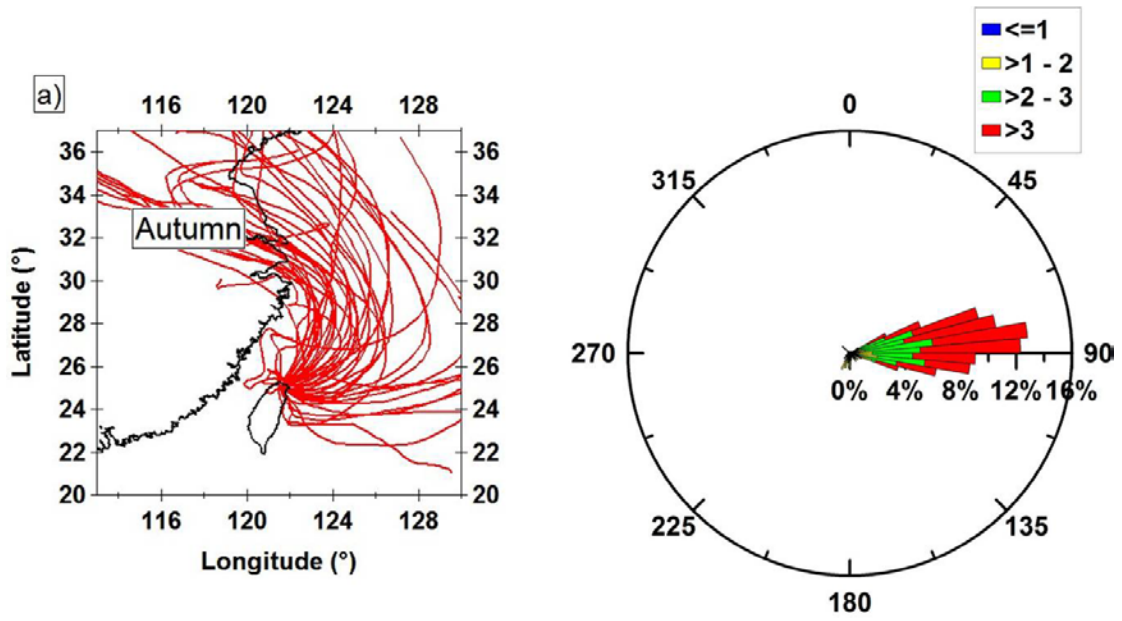
791 Wang, D., Guo, H., Cheung, K. and Gan, F. (2014). Observation of nucleation mode
792 particle burst and new particle formation events at an urban site in Hong Kong.
793 *Atmospheric Environment*, 99, 196-205.

794 Wang Z. B., Hu, M., Suu, J.Y., Wu, Z.J., Yue, D.L., Shen, X.J., Zhang, Y.M., Pei, X.Y.,
795 Cheng, Y.F. and Wiedensohler, A. (2013). Characteristics of regional new particle
796 formation in urban and regional background environments in the North China Plain.
797 *Atmospheric Chemistry and Physics*, 13, 12495-12506.

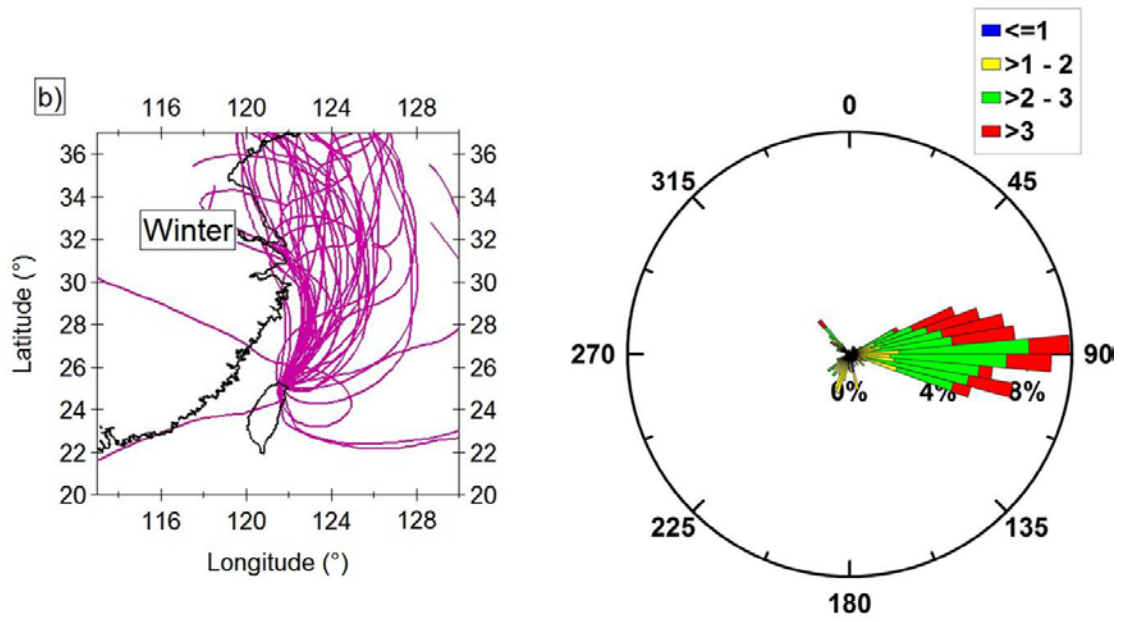
798 Woo, K.S., Chen, D.R., Pui, D.Y.H. and McMurry, P.H. (2001). Measurement of
799 Atlanta aerosol size distribution: observation of ultrafine particle events. *Aerosol*
800 *Science and Technology*, 34, 75-87.

801 Wu Z., Hu, M., Lin, P., Liu, S., Wehner, B. and Wiedensohler, A. (2008). Particle
802 number size distribution in the urban atmosphere of Beijing, China. *Atmospheric*
803 *Environment*, 42, 7967-7980.

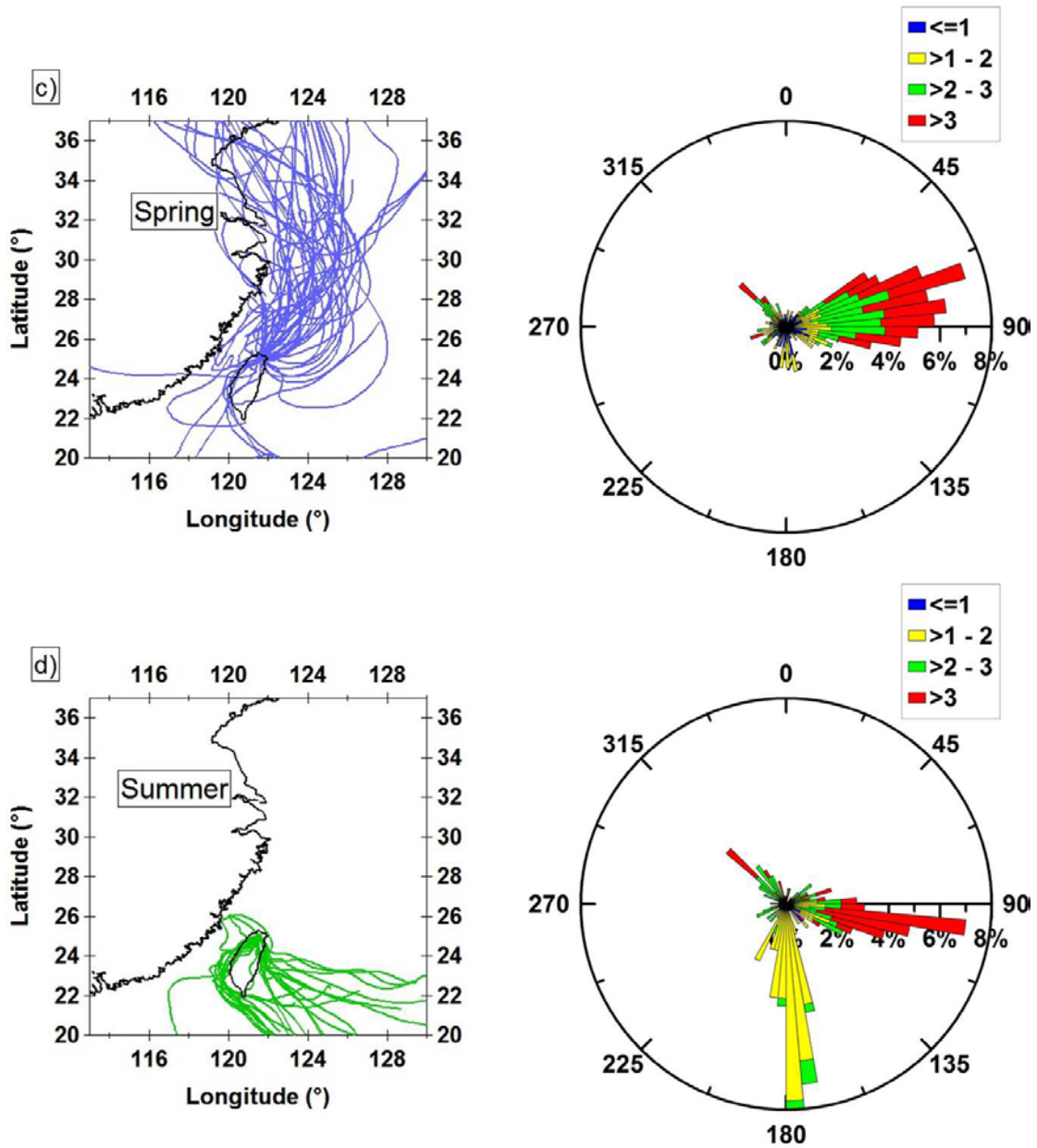
804



805



806



807

808

809

810 **Figure 1.** Back-trajectories calculated for TARO for the measurement periods (left panel) and

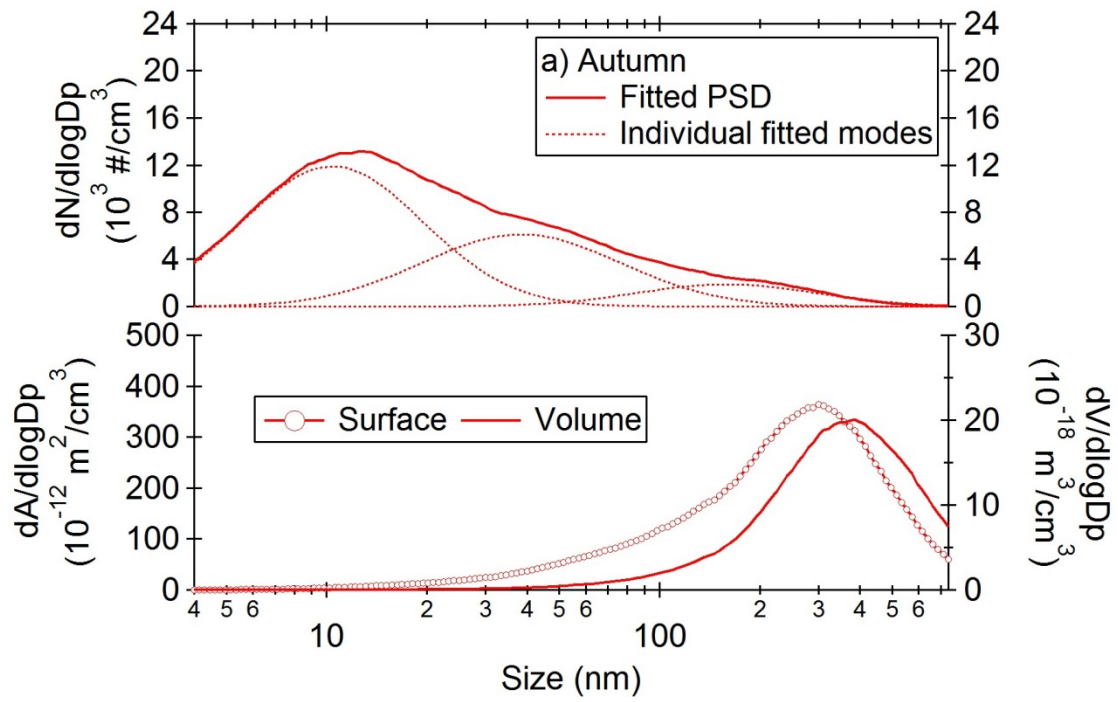
811 surface wind rose plots (right panel) in (a) autumn, (b) winter, (c) spring and (d) summer. The

812 color codes of wind rose plots represent the wind speed: blue < 1 ms⁻¹; yellow 1-2 ms⁻¹; green

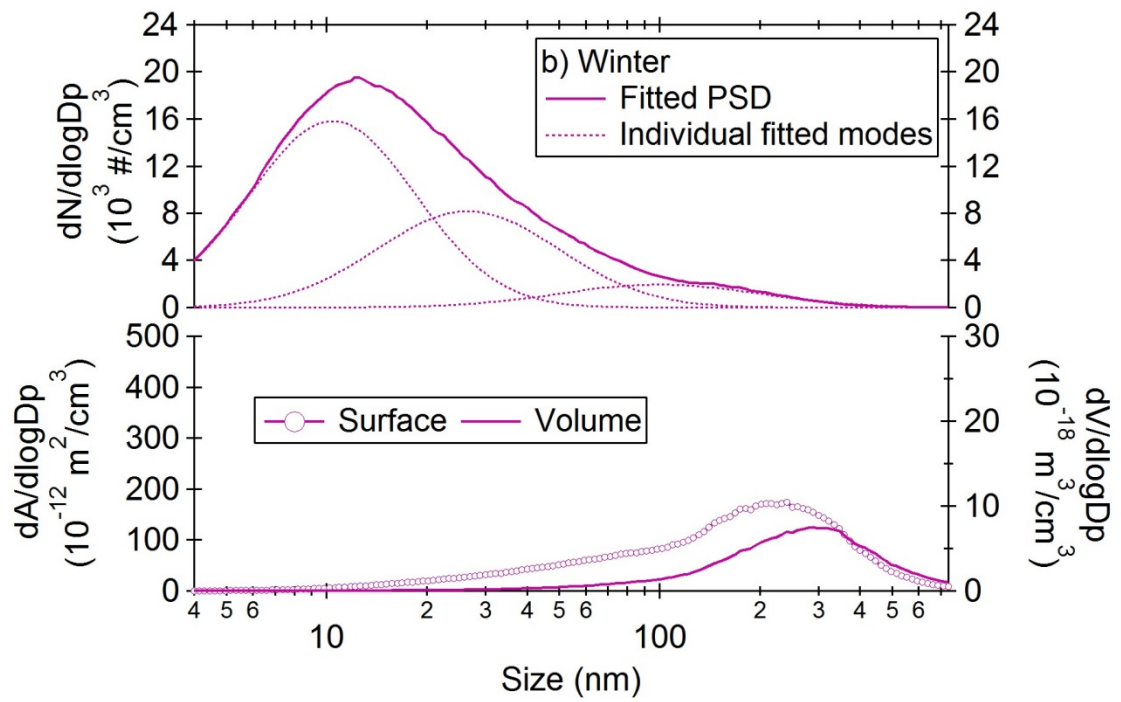
813 2-3 ms⁻¹; and red > 3 ms⁻¹.

814

815

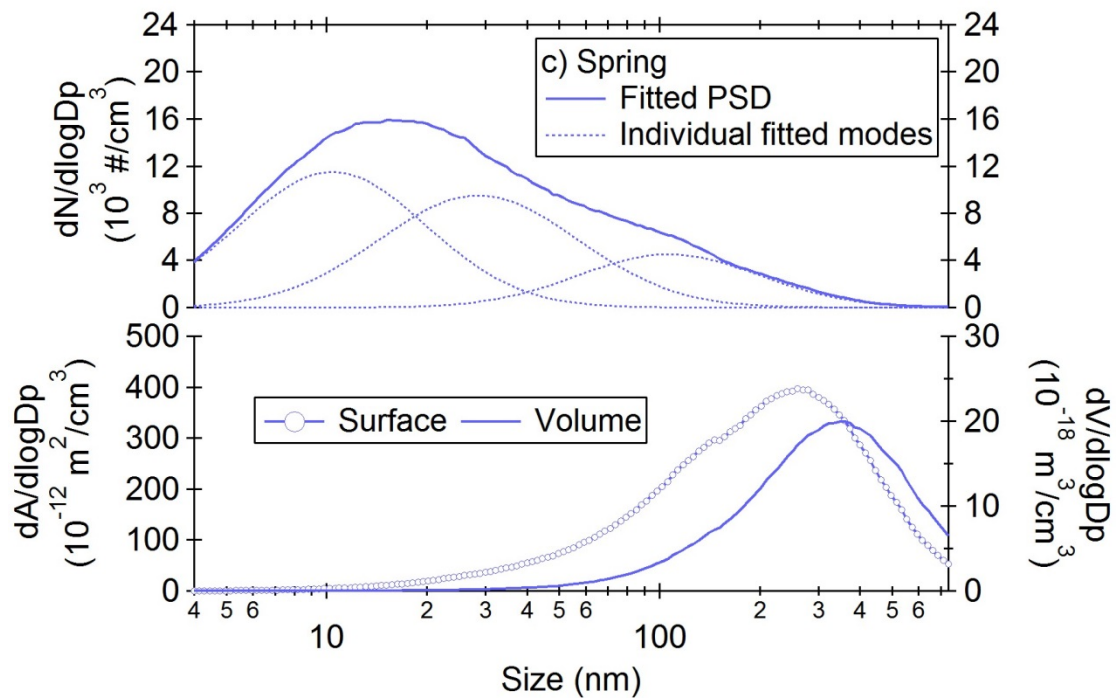


816

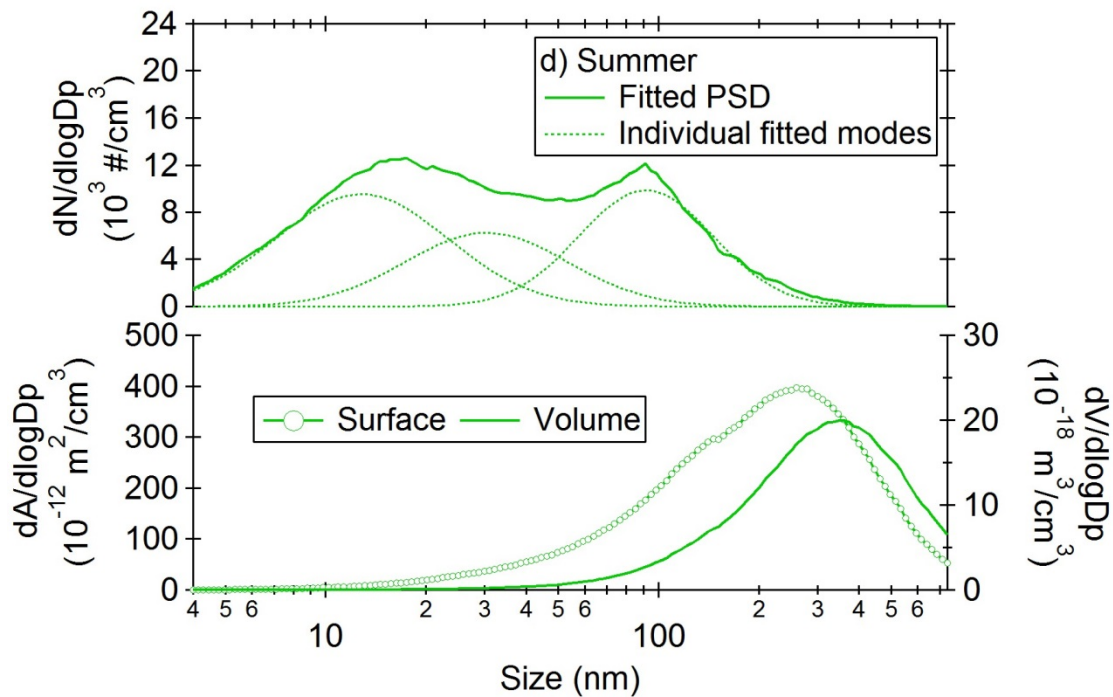


817

818



819



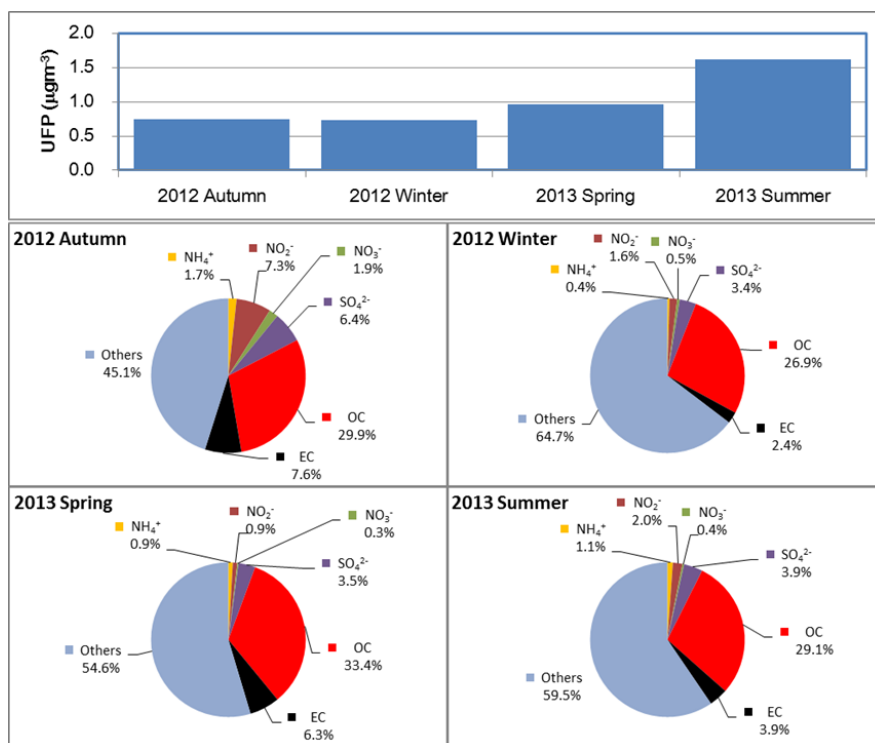
820

821

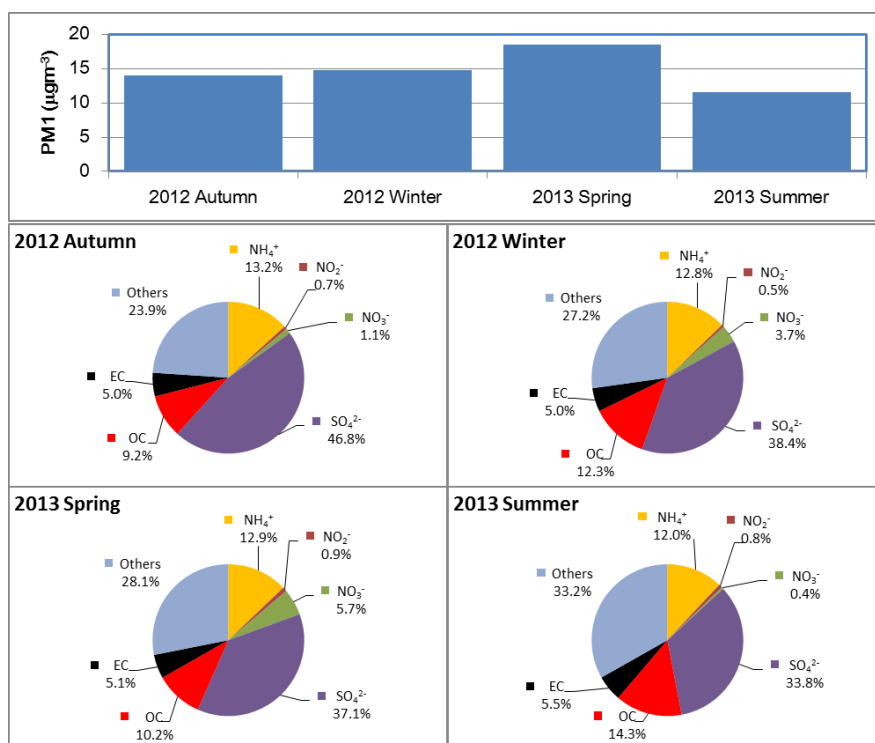
822 **Figure 2.** Size distribution of particle number (upper panel), surface and volume (lower panel)
823 concentrations measured in (a) autumn, (b) winter, (c) spring and (d) summer (by curve
824 fitting).

825

826
827



828

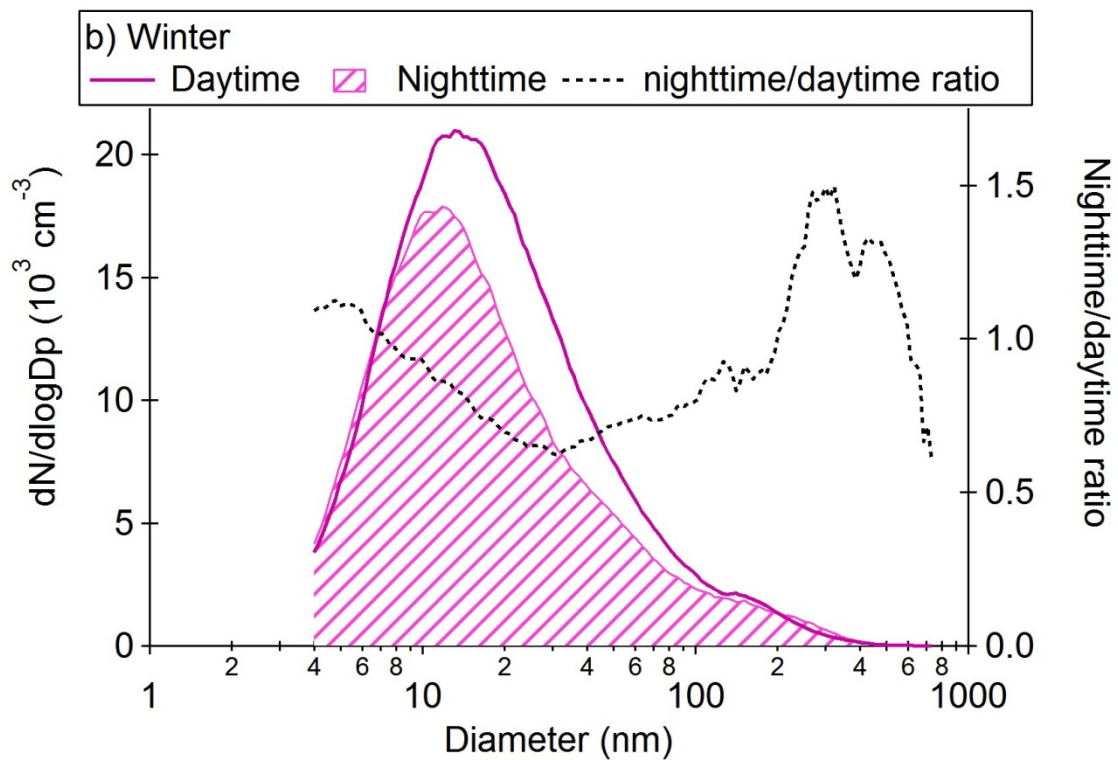
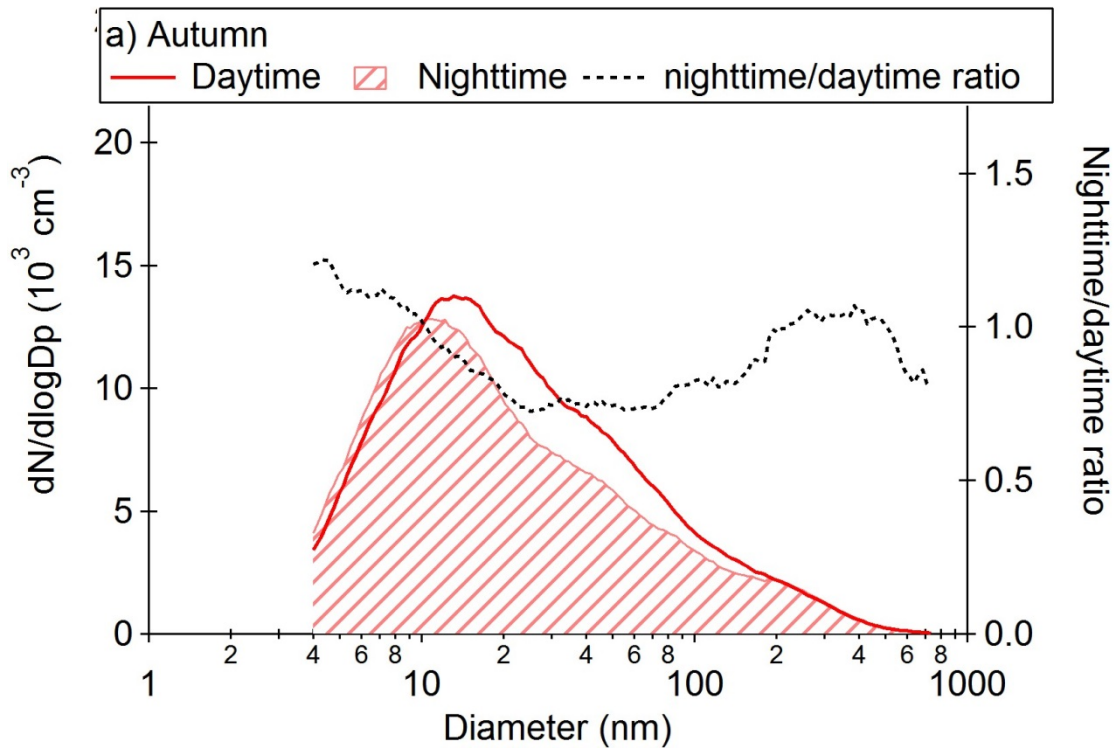


829

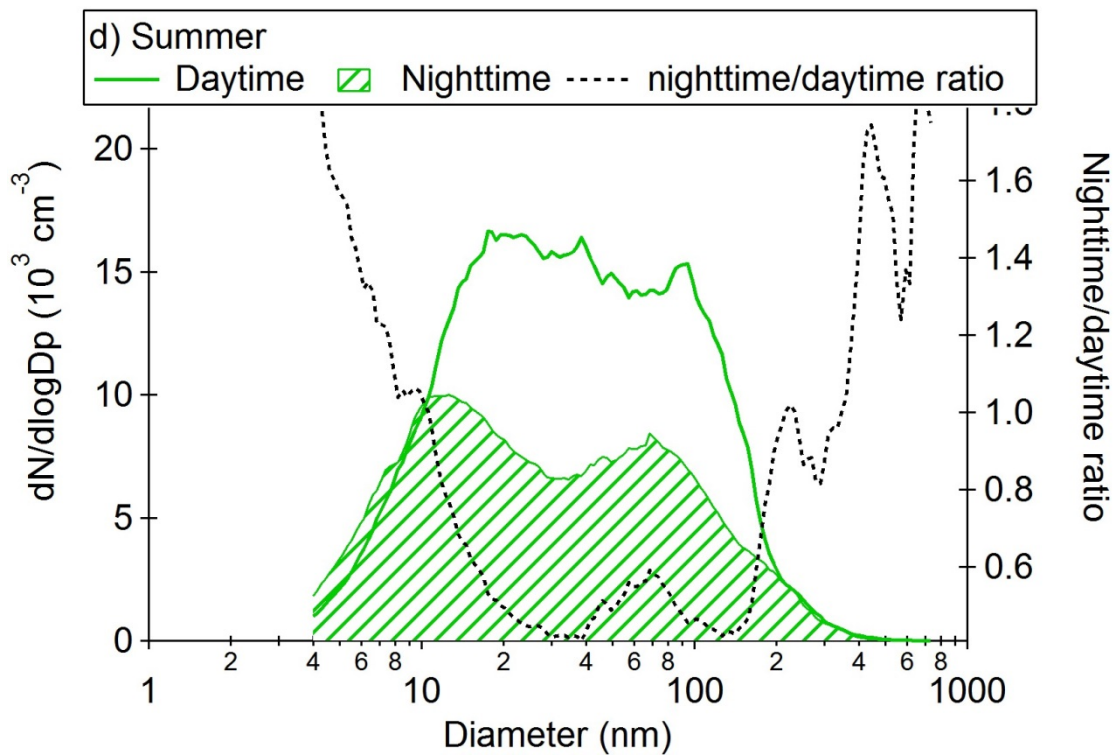
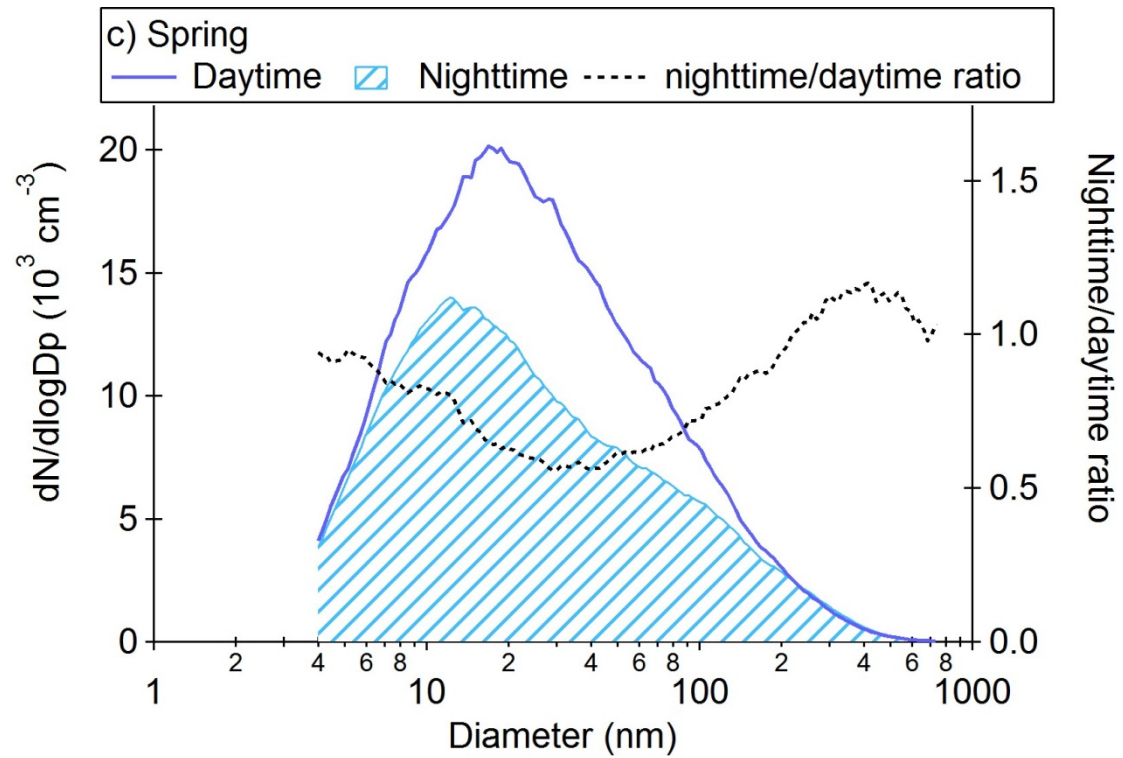
830

831 **Figure 3.** Seasonal average concentration and composition of (a) ultra-fine (UFPs) and (b)
832 sub-micron (PM₁) particles observed at the TARO in Taipei, Taiwan from autumn 2012 to
833 summer 2013.

834

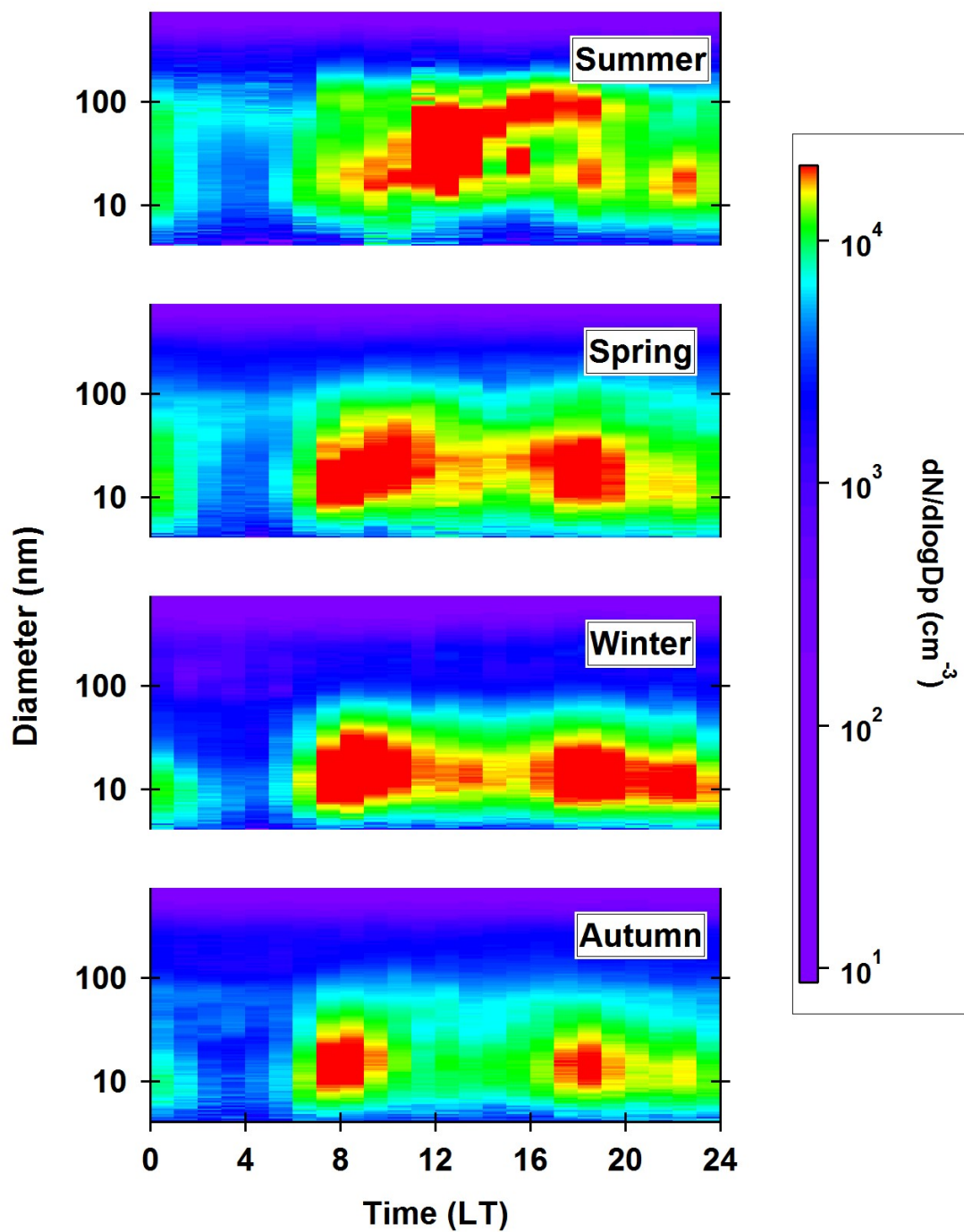


835
836
837
838
839
840
841
842



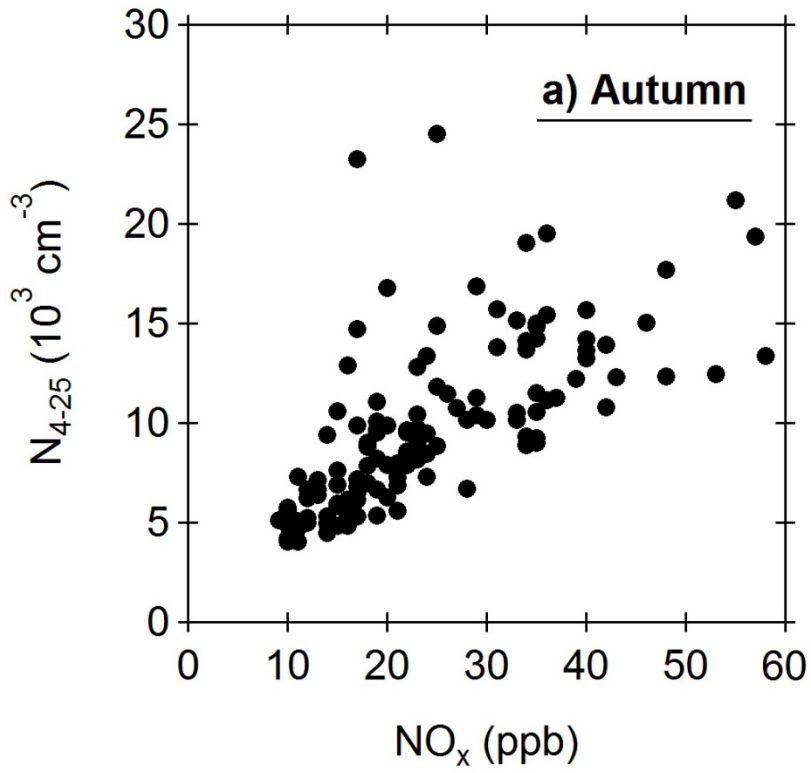
843
844
845
846
847
848
849

Figure 4. Median PSDs measured during the daytime (07:00 – 17:00 LT) and nighttime (17:00 – 07:00) in (a) autumn, (b) winter, (c) spring and (d) summer.

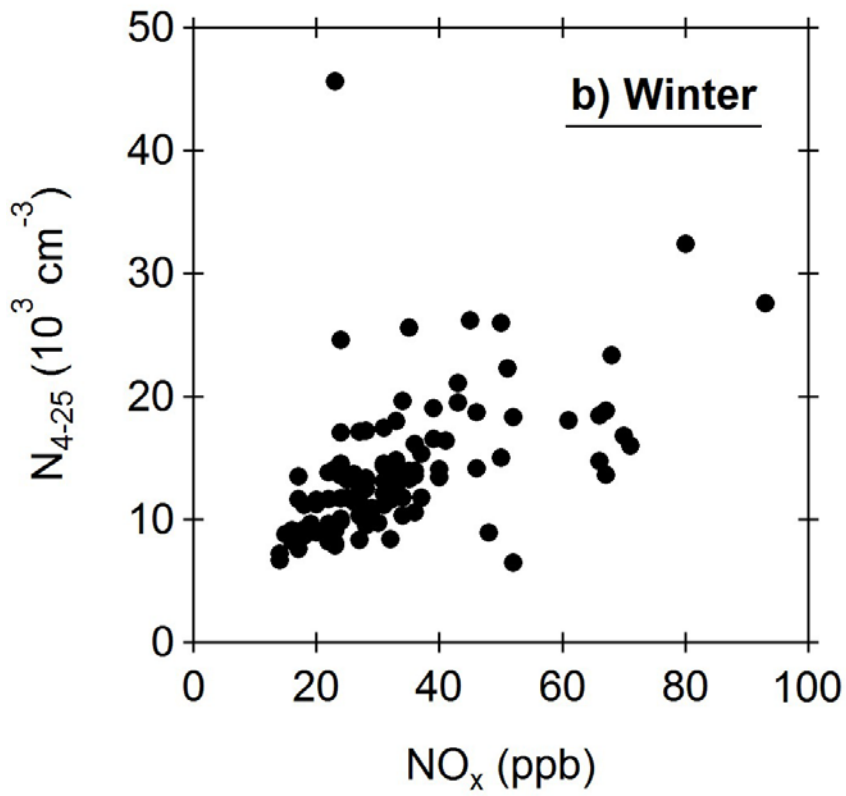


850
 851
 852
 853
 854
 855

Figure 5. Diurnal variation of particle number size distribution in each season. From lower panel to top panel: autumn, winter, spring and summer.

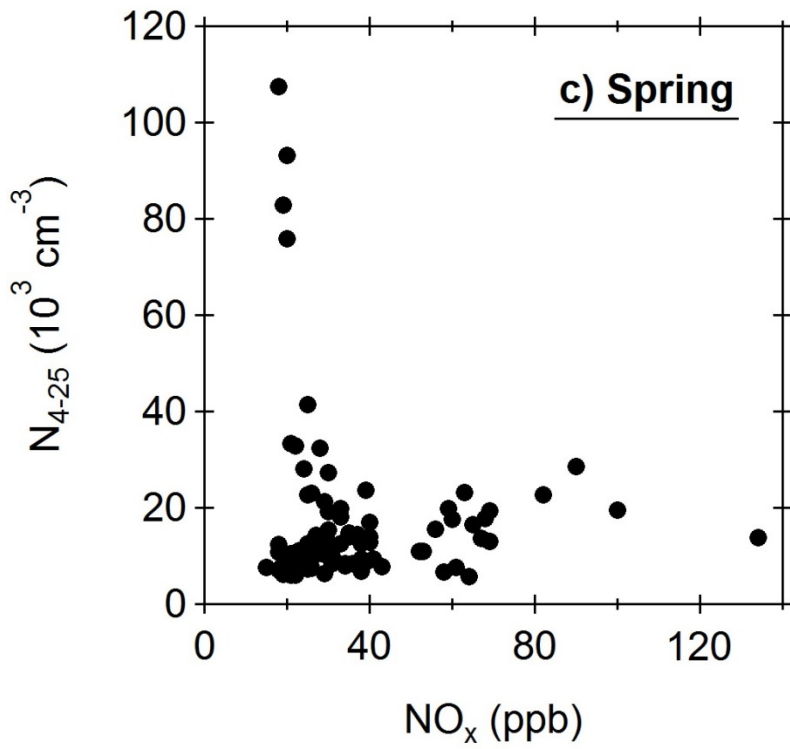


881

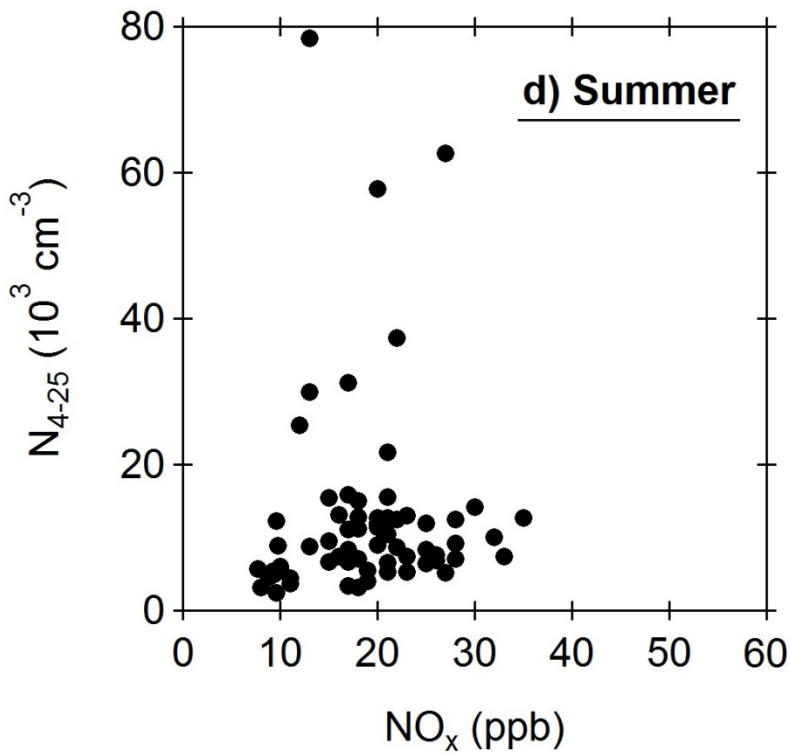


907

908
909
910
911
912



937

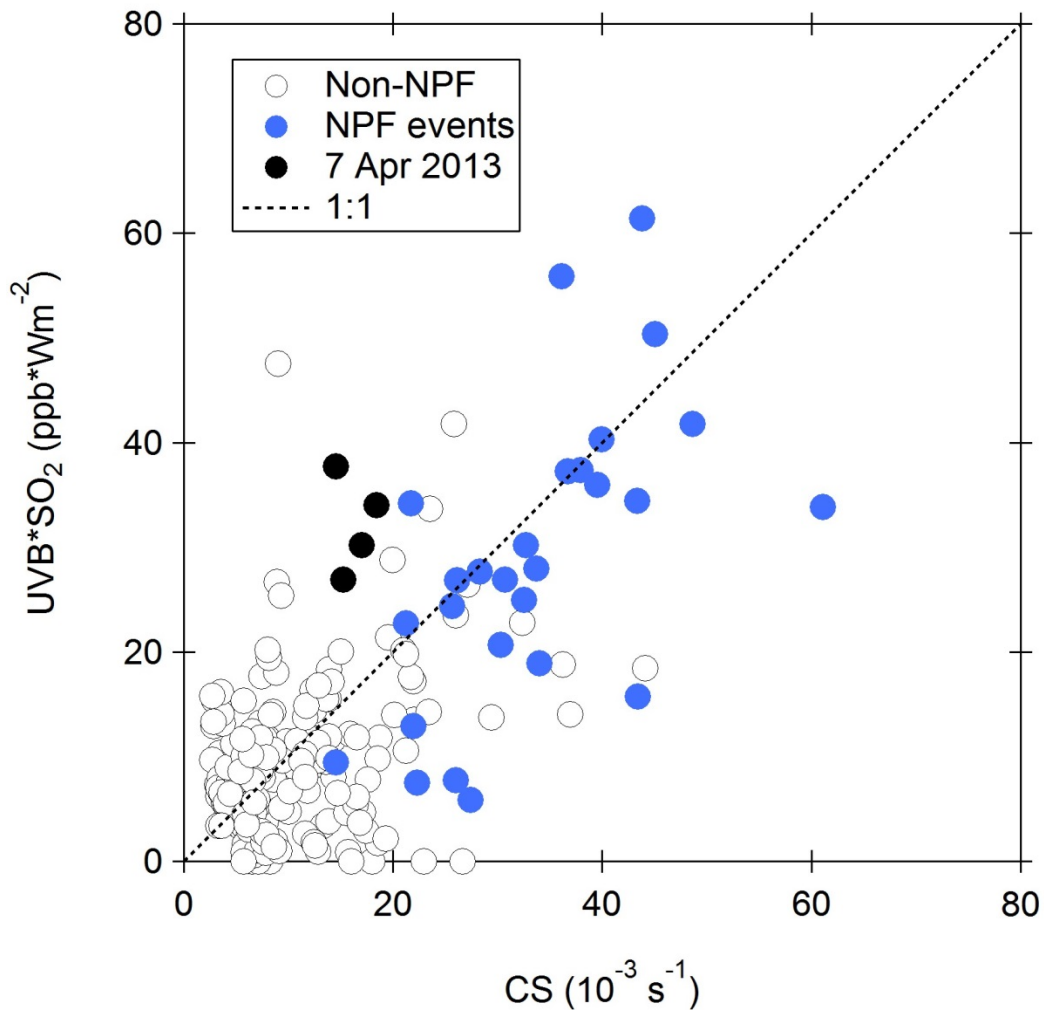


962

963 **Figure 6.** Scatter plots between hourly N_{4-25} and NO_x observed in (a) Autumn, (b) Winter, (c)
 964 Spring and (d) Summer at TARO site during the period of 07:00 – 17:00 LT.

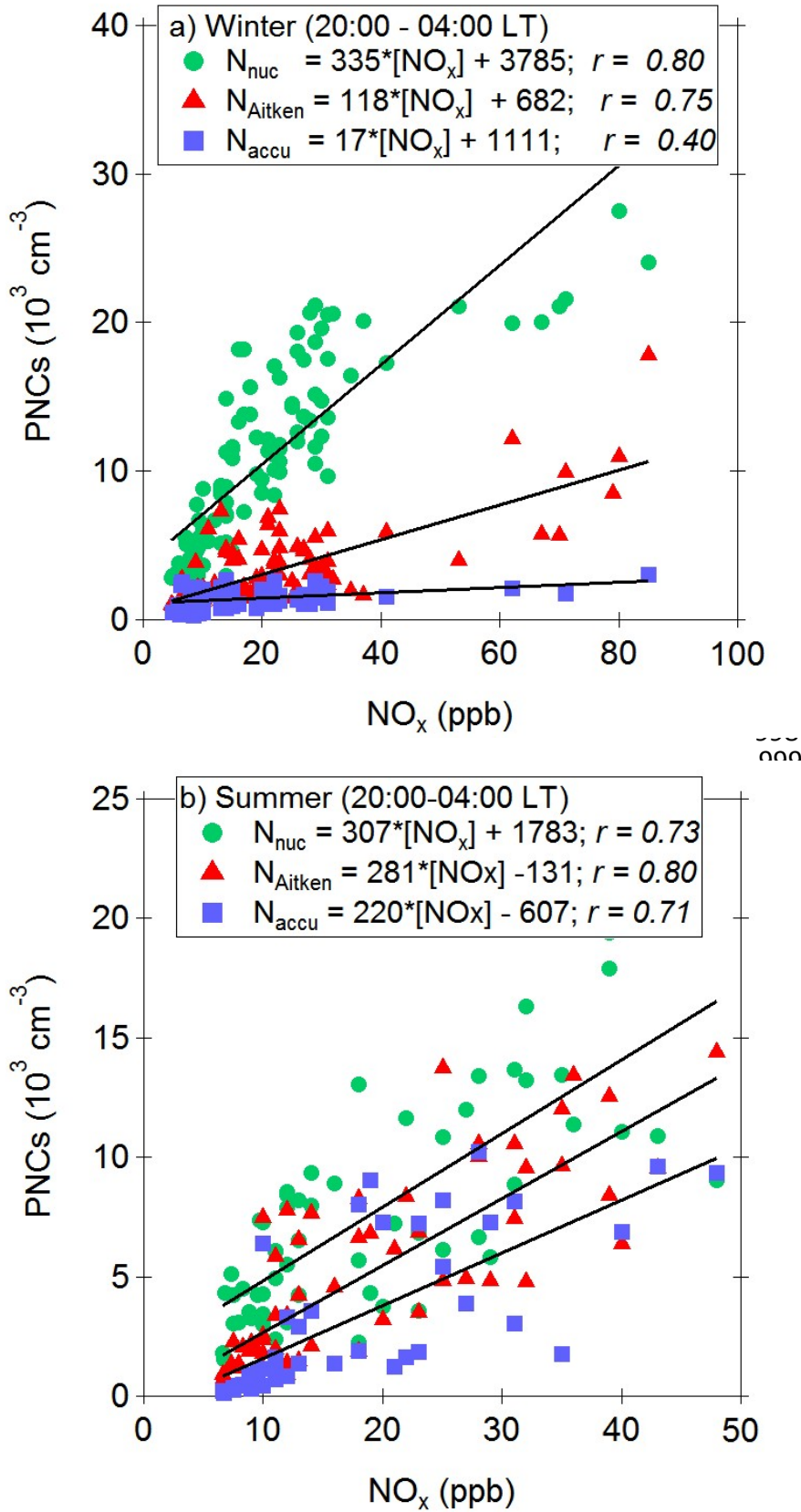
965

966



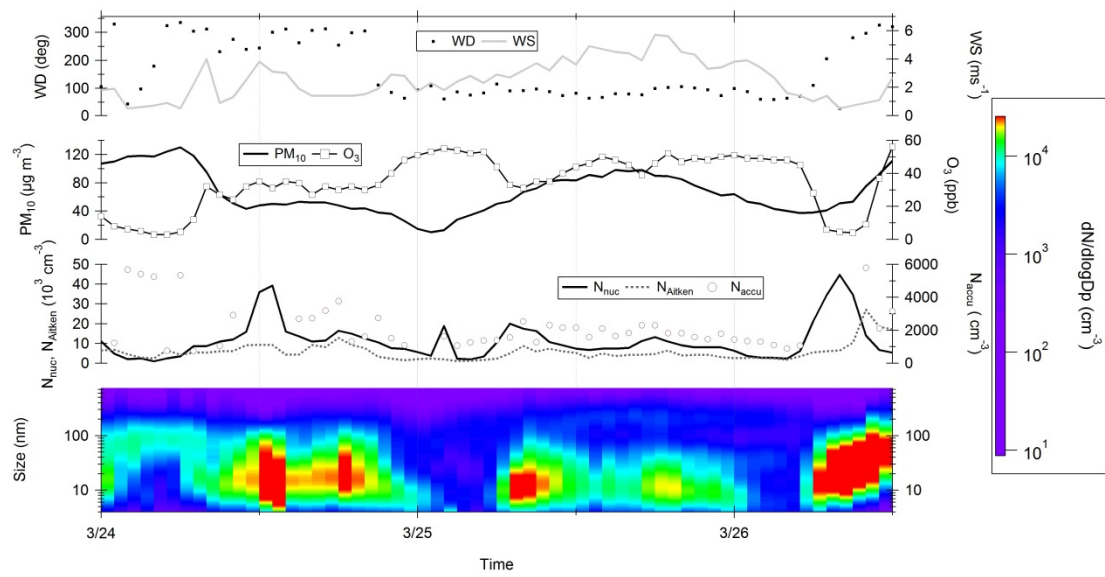
967
 968
 969
 970
 971
 972

Figure 7. Scatter plot of hourly averaged UVB*SO₂ versus condensation sink at noontime (10:00 – 14:00 LT).



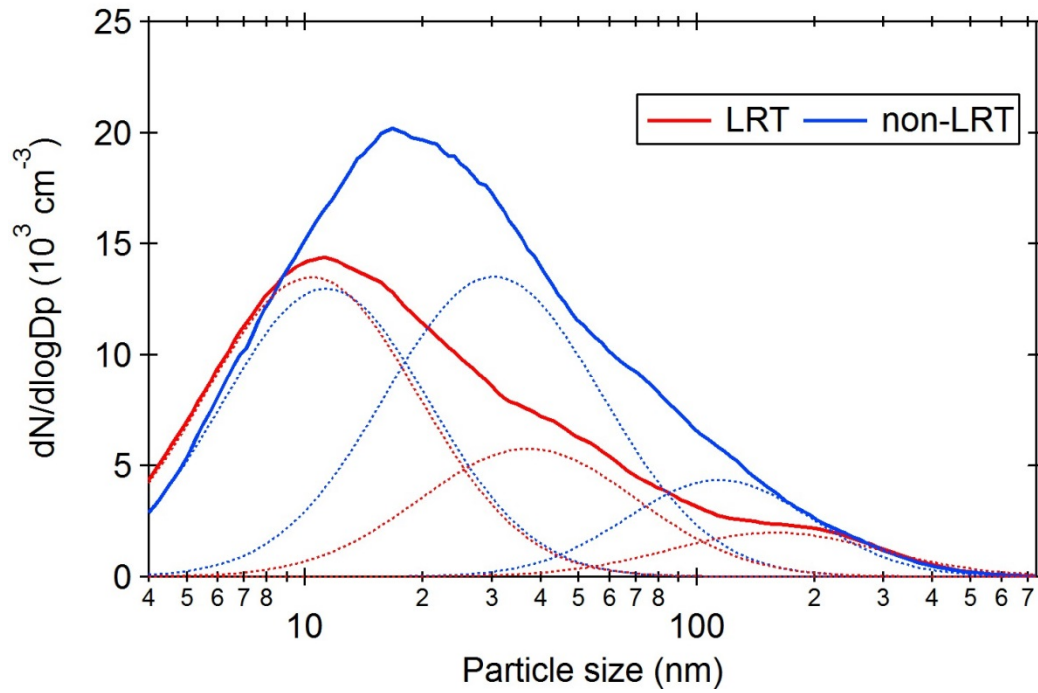
1026
 1027
 1028
 1029

Figure 8. Scatter plots for hourly averaged PNCs vs. NO_x measured during the time period of 20:00 – 04:00 (LT) in (a) winter and (b) summer, with classification of various particle size ranges.



1030
 1031
 1032
 1033
 1034
 1035

Figure 9. Time series of PSD, the N_{4-25} , N_{25-100} , $N_{100-736}$, PM_{10} , ozone (O_3) and wind direction/speed measured from 24 - 26 March 2013 (from bottom to top).



1036
 1037
 1038
 1039

Figure 10. Averaged PSDs for LRT and non-LRT episodes measured during the seasons of winter monsoons. Dashed lines illustrate the PSD of each individual mode.